



# Global Biogeochemical Cycles

## RESEARCH ARTICLE

10.1002/2017GB005787

### Key Points:

- The introduction of multiday burning into the model increases model fire interannual variability
- Historical land use change increases area burned but decreases fire emissions
- Recent land use change led to decreased global wildfire interannual variability

### Supporting Information:

- Supporting Information S1

### Correspondence to:

D. S. Ward,  
dsward@princeton.edu

### Citation:

Ward, D. S., Shevliakova, E., Malyshev, S., & Rabin, S. (2018). Trends and variability of global fire emissions due to historical anthropogenic activities. *Global Biogeochemical Cycles*, 32, 122–142. <https://doi.org/10.1002/2017GB005787>

Received 23 AUG 2017




Accepted 21 DEC 2017

Accepted article online 4 JAN 2018

Published online 17 JAN 2018

©2018. American Geophysical Union.  
All Rights Reserved.

## Trends and Variability of Global Fire Emissions Due To Historical Anthropogenic Activities

Daniel S. Ward<sup>1</sup> , Elena Shevliakova<sup>2</sup>, Sergey Malyshev<sup>2</sup> , and Sam Rabin<sup>3</sup> 

<sup>1</sup>Program in Atmospheric and Oceanic Sciences, Princeton University, Princeton, NJ, USA, <sup>2</sup>Department of Ecology and Evolutionary Biology, Princeton University, Princeton, NJ, USA, <sup>3</sup>Institute of Meteorology and Climate Research/Atmospheric Environmental Research, Karlsruhe Institute of Technology, Garmisch-Partenkirchen, Germany

**Abstract** Globally, fires are a major source of carbon from the terrestrial biosphere to the atmosphere, occurring on a seasonal cycle and with substantial interannual variability. To understand past trends and variability in sources and sinks of terrestrial carbon, we need quantitative estimates of global fire distributions. Here we introduce an updated version of the Fire Including Natural and Agricultural Lands model, version 2 (FINAL.2), modified to include multiday burning and enhanced fire spread rate in forest crowns. We demonstrate that the improved model reproduces the interannual variability and spatial distribution of fire emissions reported in present-day remotely sensed inventories. We use FINAL.2 to simulate historical (post-1700) fires and attribute past fire trends and variability to individual drivers: land use and land cover change, population growth, and lightning variability. Global fire emissions of carbon increase by about 10% between 1700 and 1900, reaching a maximum of 3.4 Pg C yr<sup>-1</sup> in the 1910s, followed by a decrease to about 5% below year 1700 levels by 2010. The decrease in emissions from the 1910s to the present day is driven mainly by land use change, with a smaller contribution from increased fire suppression due to increased human population and is largest in Sub-Saharan Africa and South Asia. Interannual variability of global fire emissions is similar in the present day as in the early historical period, but present-day wildfires would be more variable in the absence of land use change.

### 1. Introduction

Global biomass burning is a source of roughly 2.5 Pg of carbon to the atmosphere annually (Randerson et al., 2012; van der Werf et al., 2010), making fires a major component of the terrestrial carbon balance and an important contributor of atmospheric trace gas and aerosol constituents with associated climate impacts (e.g., Jacobson, 2014; Naik et al., 2007; Ward et al., 2012). To understand the sources and sinks of carbon in the terrestrial biosphere historically, the past trends and variability in global fires need to be estimated quantitatively. Charcoal sediment records suggest that regional fire dynamics are characterized by long term (decade to century scale) trends, including a pronounced increase in fires from 1700 to the late 1800s, followed by a decrease lasting through the middle to late twentieth century (Marlon et al., 2016; van der Werf et al., 2013). Efforts to reconstruct twentieth century global fires using other proxies or modeling do not agree on the sign of the trend (e.g., Mouillot & Field, 2005; Yang et al., 2014) and are complicated by the increase in agricultural and deforestation burning in recent decades (Kloster et al., 2010).

Historical (post-1700) trends in global fire emissions are thought to result from changes in climate, changes in land cover and land use, and changes in human population and associated ignition and fire suppression activities. Yue et al. (2015) found a positive response in global wildfires to twentieth century climate changes, despite excluding agricultural and deforestation fires in their study, consistent also with the results of Knorr et al. (2016). The role of human population in driving global fire trends contains many uncertainties, especially regarding the relative importance of ignition, suppression, and land use. The substantial historical decrease in modeled fires shown by Knorr et al. (2014, 2016) is attributed to increasing population, while earlier work by Kloster et al. (2010, 2012) found no trend in historical or projected global fires due to population change. Bistinas et al. (2014) use a statistical model developed from present-day data sets to suggest fire suppression dominates under increasing human population but do not claim a causal relationship due to the lack of independence between model factors. The impact of land cover changes on fire activity is similarly difficult to isolate from other drivers (Pechony & Shindell, 2010), but most studies have found that historical land use and land cover changes have decreased fires globally (Andela et al., 2017; Houghton et al., 1999; Kloster et al., 2012; Ward & Mahowald, 2015; Yang et al., 2014).

Fire activity is also affected by both changes in the distribution of plant species in an ecosystem, such as the introduction of nonnative grasses in the western United States (Balch et al., 2013), and regional trends in lightning strikes (Krause et al., 2014). The importance of these different factors for driving trends in fire activity, in addition to being uncertain on a global scale, is not consistent between regions of the world because of different ecology and fire management strategies (e.g., Bistinas et al., 2013; Kloster et al., 2010).

While modeling studies of global fires often focus on trends, less attention is given to the interannual to decadal variability of global fires, although it is well established that emissions of carbonaceous aerosols and trace gases from global fires vary substantially on an interannual basis (van der Werf et al., 2006, 2010). Estimated global, annual fire emissions range between 1.8 Pg C yr<sup>-1</sup> to 3.0 Pg C yr<sup>-1</sup> for the 20 year period between 1997 to 2016 (Giglio et al., 2013). While fossil fuel burning emits more carbon on a global basis, the year-to-year variations in natural fire emissions are large enough to cause notable changes in the global CO<sub>2</sub> growth rate (Nevison et al., 2008). Fires are also responsible for much of the observed interannual variability (IAV) in global CO and carbonaceous aerosol concentrations, with consequences for year to year changes in regional climate and air quality (Voulgarakis et al., 2015) and are a major contributor to IAV in arctic snowmelt rate (Flanner et al., 2007).

Given the short satellite record available for fires, the large IAV of global fires limits our ability to detect a climate change signal in global fire emissions (Doerr & Santín, 2016; Giglio et al., 2013; Ward et al., 2016). Global fire models are used to improve our understanding of fires responses to changes in climate, population, and land cover before the satellite record (Hantson et al., 2016). However, many of these models simulate only average quantities over long time periods and on coarse horizontal grids and do not capture variations in regional emissions from year to year. On a regional basis, year-to-year variations in fires impact issues of air quality (e.g., Lelieveld et al., 2015; Real et al., 2007; Reddington et al., 2014; Voulgarakis & Field, 2015) and landscape management (e.g., Adams, 2013; Millar & Stephenson, 2015). Grandey et al. (2016) found that the global radiative effects from fire aerosols are overestimated by 0.2 W m<sup>-2</sup> when interannual variability in emissions is neglected. The impact of neglecting the year to year variations on in radiative forcing is especially strong for boreal emissions (Clark et al., 2015; Grandey et al., 2016).

Global emissions variability is driven mainly by regional events in extratropical forests and in some tropical areas where variability is associated with tropical sea surface temperature oscillations (van der Werf et al., 2006). For example, fires in Indonesia in 1997–1998, responding to the concurrent major El Niño event and primed for drought by recent land use, caused a noteworthy increase in the rate of global CO<sub>2</sub> growth (van der Werf et al., 2004). High IAV is also characteristic of fires in Central America and boreal regions due to climate variability (Giglio et al., 2013).

While some global fire models capture the IAV and extremes in equatorial Asia fire emissions, IAV in boreal fires has proven to be comparatively challenging to simulate (e.g., Kloster et al., 2010; Li et al., 2012; van Marle et al., 2017; Ward et al., 2016). Annual fire emissions in these northern forests depend greatly on the frequency of occurrence of extreme fires. Sometimes referred to as “megafires,” these can burn for weeks to months, are often characterized by crown burning and associated enhanced fire spread rates, and account for a large percentage of the burned area and emissions for a given fire season (Flannigan et al., 2009). The potential for megafires in boreal North America is enhanced by favorable climate conditions, such as drought, preceded by a wet year that boosts fuel availability (Abatzoglou & Kolden, 2013), although it is possible to have extreme fires during years without a conducive climate (Lannom et al., 2014). Infrequent, long-duration fires present a particular challenge to global fire models, which do not typically simulate individual fire events and often use a fixed fire duration. Models that allow multiday burning produce more realistic fire IAV in boreal regions (e.g., Le Page et al., 2015; Pfeiffer et al., 2013). HESFIRE (Human-Earth System FIRE) (Le Page et al., 2015) includes both multiday burning and fire intensity dependent fire rate of spread (ROS) and is capable of reproducing observed boreal fire emission IAV, although it exhibits a low bias in annual emissions in these regions. Yue et al. (2014) developed an offline method to concatenate fixed-duration model fires into multiday fires that leads to realistic boreal fire IAV despite an underrepresentation of extreme large fires in the fire size distribution.

In this study we describe several model improvements, including the addition of multiday fires, to the Fire Including Natural and Agricultural Lands, version 2 (FINAL2) global fire model (Rabin et al., 2017) coupled with the NOAA-Geophysical Fluid Dynamics Laboratory (GFDL) land model (LM3), with a view toward

improving the model representation of global and regional fire emission IAV. Specifically, we aim to reduce the biases in boreal region area burned and in global fire IAV noted by Rabin et al. (2017). We compare the model performance in the present day to available inventories of global fire characteristics, noting that the model's ability to capture observed global IAV provides an important test of its response to changes in climate. We then apply FINAL.2 with these developments in simulations of the historical time period (1700 to 2010) to estimate past trends in global and regional fires. With the results of these simulations we also assess the importance of historical land use and land cover change and human population change for the IAV of global fire emissions, and implications for projections of future fires.

## 2. Methods

The Fire Including Natural and Agricultural Lands model (FINAL) was introduced into the GFDL global terrestrial model LM3 (Malyshev et al., 2015; Milly et al., 2014; Shevliakova et al., 2009) by Rabin et al. (2017). The natural fire scheme in FINAL is based on Li et al. (2012, 2013), a process-based fire model that predicts area burned from grid-scale fuel availability, fuel moisture, and ignition sources (Arora & Boer, 2005; Kloster et al., 2010, Li et al., 2012). Li et al. (2012, 2013) introduced prediction of fire occurrence to the framework of the previous schemes, formulated as a product of ignition events, and functions of fuel moisture, fuel availability, environmental temperature and relative humidity, and human fire suppression. The fire spread forms an elliptical shape according to the wind speed forcing, and modified by soil and atmospheric moisture factors. A maximum fire rate of spread (ROS) is applied with values dependent on vegetation type (Li et al., 2013) and characteristic of surface fire spread, not including the faster ROS associated with crown fire. Rabin et al. (2017) adopted a maximum fire size for FINAL based on the work of Pfeiffer et al. (2013), designed to reproduce the effects of landscape fragmentation on fire spread. The fire ROS determines the burned area per fire occurrence, which is multiplied by the number of fires to give the total burned area for a given model day.

Li et al. (2013) applied the same fire scheme to both unmanaged and managed lands such as pastures. Agricultural fires, including burning of crop residue and pasture fires, are prescribed in FINAL according to the data and methodology of Rabin et al. (2015). Pasture fires in particular were shown to comprise a large percentage of present-day global burned area in FINAL (40 to 50%) and in Global Fire Emissions Database version 3 with small fires (GFED3s) (Randerson et al., 2012) when separated into agricultural and nonagricultural fires (Rabin et al., 2017). Most present-day agricultural fires occur in the tropics, but they also dominate in areas of Eastern Europe. Agricultural fires depend on crop and pasture area in FINAL, but not on environmental changes and, therefore, act to reduce the IAV of the modeled fires. Emissions are computed by applying vegetation-type-dependent combustion completeness factors to the aboveground biomass in the burned areas. Separate values are used for leaf, stem, and litter biomass and follow those given by Li et al. (2012).

### 2.1. Crown Fire Spread

Fires that burn with sufficient intensity on a forested landscape with a closed canopy can spread from the surface to the forest crown (Rothermel, 1991). Crown fires are observed most often in boreal forest biomes (Archibald et al., 2013) and, due to differences in species composition, are more common in North America than in Eurasia (Rogers et al., 2015). These fires are characterized by enhanced intensity and ROS (Rothermel, 1991) and are a common component of megafires (Stephens et al., 2014). The limitations on ROS in the initial version of FINAL (FINAL.1) are independent of fire type and characteristic of surface fires (Li et al., 2012). Here we introduce an enhanced fire ROS for instances of high-intensity fires to better represent the impacts of crown fires in the new version of FINAL (FINAL.2).

We predict crown fires in FINAL.2 following the methodology of Thonicke et al. (2010) that first requires a calculation of the fire intensity. As in SPITFIRE (SPread and InTensity of FIRE) (Thonicke et al., 2010), the surface fire intensity, more specifically the fire line intensity,  $I_{sfc}$  ( $\text{kW m}^{-1}$ ), is computed as a product of the fuel consumption FC ( $\text{kg}_{\text{dry matter m}^{-2}}$ ), fire rate of spread  $\text{ROS}_{sfc}$  ( $\text{m s}^{-1}$ ), and a constant fuel heat content  $h$  ( $18,000 \text{ kJ kg}_{\text{dry matter}}^{-1}$ ):

$$I_{sfc} = h \times \text{FC} \times \text{ROS}_{sfc} \quad (1)$$

The rate at which biomass is consumed by a wildfire depends on the class of the fuel being burned. Thonicke et al. (2010) define four fuel classes characterized by the lag between changes in ambient moisture content and fuel moisture content, measured in hours: 1 h, 10 h, 100 h, and 1,000 h. Generally, smaller diameter fuels

respond more quickly to atmospheric conditions and comprise the 1 h and 10 h classes. The three fuel classes with the shortest moisture response lag time (1 h, 10 h, and 100 h) are used to compute the FC and contain 4.5%, 7.5% and 21% of hardwood and sapwood C, respectively, in SPITFIRE (Thonicke et al., 2010). The FC of each fuel class is determined in SPITFIRE using a set of rules based on the ratio of fuel moisture content,  $\omega_o$ , to the moisture of extinction,  $m_e$  ( $m_e = 0.69$ , Thonicke et al., 2010). In LM3, litter pools are not distinguished by fuel class. Instead, we derive a relationship between FC and total litter carbon by first averaging the FC rules for the 1 h, 10 h, and 100 h fuel classes described in Thonicke et al. (2010), weighted by their carbon content, across 100 values of  $\omega_o$  between 0 and 1. We then fit a logarithmic function to the FC values by minimizing the root-mean-square error:

$$FC = [\ln(\omega_o/m_e + 0.63) + 0.47] \times DM \quad (2)$$

where DM is the dry matter fuel content (kg), calculated as the total litter carbon divided by 0.45, which is often used as the carbon:DM fuel ratio (e.g., Lamarque et al., 2010; Ward et al., 2012). The fuel moisture content,  $\omega_o$ , is computed in FINAL. The fire line intensity can be used to determine the fraction of fires in a grid box that reach the crown by first calculating the fire scorch height, SH (Thonicke et al., 2010):

$$SH = F \times I_{sfc}^{0.667} \quad (3)$$

where  $F$  is a plant functional type (PFT)-dependent scorch height parameter, given for different PFTs in Thonicke et al. (2010).  $F$  is zero for grass PFTs, eliminating crown fire for grasslands regardless of the fuel consumption. The crown scorch fraction, CK, is determined by comparing the SH to the average vegetation stand height:

$$CK = (SH - H + CL)/CL \quad (4)$$

where  $H$  is the average stand height (computed online within LM3) and CL is the crown length, a PFT-specific parameter for which we use the values given in Thonicke et al. (2010). CK is set to zero when SH or  $H$  is equal to zero. Here we use the CK predicted in FINAL to represent the fraction of fires (measured by fire number) that reaches the crown and experiences enhanced ROS as a result. While wind speed-dependent crown fire ROS models have been developed (e.g., Cruz et al., 2005), here we take a simpler approach. Rothermel (1991) developed an empirical relationship between surface fire ROS and crown fire ROS from observations in the northern Rocky Mountains, finding an average crown fire enhancement of 3.34 times the surface fire ROS. We use this enhancement factor for crown fires in FINAL.2, modifying the fire ROS to account for the CK as follows:

$$ROS = ROS_{sfc} \times (1 - CK) + ROS_{sfc} \times (CK) \times 3.34 \quad (5)$$

Cruz et al. (2005) found that using the Rothermel (1991) results leads to underpredicted ROS compared to observed Canadian fires, meaning our ROS enhancement for crown fires may be considered conservative.

## 2.2. Multiday Burning

Fires represented in FINAL.1 burn for 24 h, as in Li et al. (2012), regardless of model environmental conditions. This simplification of multiday fires, which can burn for months at a time (e.g., Running, 2006; Wang et al., 2014) and even smolder through the winter season under snow cover to spark new fires in the spring (Flannigan et al., 2009), may be sufficient for simulating fires on an annual average but is limiting for addressing questions of fire IAV and changes in future fire activity. Fire duration itself may change with the warming global climate, possibly increasing by up to a factor of 2 to 3 in Canada (Wang et al., 2017).

To account for the occurrence of multiday fires, we allow fire duration to increase by 1 day for every 24 h period that passes without an “extinguishing” time step. A maximum duration of 30 days is imposed on all fires for computational efficiency. This follows from similar schemes in which the number of fires on a given day is the sum of fires initiated that day and fires from previous days that have not been extinguished (e.g., Le Page et al., 2015; Pfeiffer et al., 2013). Extinction occurs when the conditions to support fire initiation fall below a threshold value (defined below) at any time step in a particular grid cell. At such a time step all currently burning multiday fires in that grid cell are extinguished. The multiday fire scheme does not impact the number of fires initiated, or the rate of spread parameters for a given day, and the burned area per fire ( $BA_{pf}$ ) is computed using the same formula as for initial-day fires (Rabin et al., 2017):

$$BA_{pf} = \frac{\pi \times (ROS_f \times d)^2}{4 \times 10^6 \times LB} \times (1 - HB^{-1})^2 \quad (6)$$

where  $BA_{pf}$  is in units of square kilometers,  $ROS_f$  is the fire rate of spread ( $m s^{-1}$ ),  $d$  is the fire duration (s), and  $LB$  and  $HB$  are the length:width and head:back ratios of the elliptical fire burn scar, respectively.

When fires are allowed to burn for multiple days, the size of the initial burn perimeter increases and the areal consumption of the fire will proceed at a higher rate for the same ROS, compared to a fire beginning at an ignition point. Moreover, the additional area burned on day  $n$  (subsequent to the ignition event) depends on the area of the fire at the beginning of the day, which is the accumulated area burned over several days with different spread rates. We alter the fire duration,  $d_{n(adj)}$ , in equation (6) to account for the nonlinear expansion rate of the elliptical fire on days subsequent to the ignition day:

$$d_{n(adj)} = \sqrt{\frac{BA_{n-1} \times d_{1day}^2}{N_{n-1} \times BA_{pf(ave)}}}$$

where  $BA_{n-1}$  is the total area burned by the multiday fire by 24 h prior to this calculation,  $N_{n-1}$  is the number of multiday fires burning during the previous 24 h, and  $d_{1day}$  is a burning duration of 1 day (86,400 s). This expression also uses the burned area per fire computed using the average ROS and fire shape parameters ( $LB$  and  $HB$ ) from the previous 24 h ( $BA_{pf(ave)}$ ). The  $d_{n(adj)}$  represents the age of the fire that would lead to the current total area burned given the previous day's rate of spread. In this way, if the fire grows slowly for a few days but the rate of spread is suddenly increased in the 24 h prior to the new  $BA_{pf}$  calculation, the added burned area will begin from the actual fire size, thereby accounting for the different daily rates of spread.

To compute the additional area burned in a day by a multiday (nonextinguished) fire ( $BA_{pf(n)}$ ), the  $BA_{pf(ave)}$  is computed using the adjusted duration and the  $BA_{n-1}$  is subtracted to give the additional area burned during that day:

$$BA_{pf(n)} = \left( BA_{pf(ave)} \times \frac{d_{n(adj)}}{d_{1day}} \right) - BA_{n-1}$$

As fires last longer and grow bigger, they consume greater and greater fractions of the initial model tile area, and allowance needs to be made for the increased likelihood that fires will merge, reducing the number of fires. We estimate the coalescence of fires from the results of a simple model that places elliptical shapes at random locations on a fixed-size, square grid. Approximately 1,000 iterations of this model with different  $LB$ , ellipse areas, and ellipse number give a distribution of number of ellipse mergings and the fraction of grid area covered by ellipses. The results were not sensitive to the  $LB$  of the ellipses. For multiday fires, fire coalescence reduces the fire number to an "adjusted fire number" ( $N_{adj}$ ) according to a function fit to the results from this simple model by minimizing the root mean squared error:

$$N_{adj} = N_{mdf} \times \left( 1 - \frac{BA_{mdf}}{A_{mdf}} \right)^2$$

where the subscript mdf indicates multiday fire and  $A_{mdf}$  is the tile size associated with the day the fires began. The size of the tile during the initial day of the fire is tracked throughout the total life of the fire, so daily reductions in tile area from fires do not artificially inflate coalescence rates.

Multiday fires will continue to expand as long as conditions support formation of a threshold number of fires per day (calculated every time step), similar to a "stopping rule" used for determining the end of a drought for computing drought indices (Keyantash & Dracup, 2002). This threshold value ( $f_{ext}$ ) is calculated using the existing formula for fire occurrence in FINAL.1 and FINAL.2 with a constant ignition rate ( $10^{-5}$  ignitions  $km^{-2}$ ) to allow for sustaining already-burning fires in the absence of ignition events. The impact of the ignition-independent threshold calculation is negligible for the current model setup in which anthropogenic ignitions change yearly, and natural lightning ignitions change only on a monthly basis. However, this would become highly relevant for future applications which may include daily lightning or lightning calculated online within an Earth System model.

The average duration of multiday fires in this new scheme is tested for  $f_{ext}$  values of 0.5, 1, 3, and 5 fires per day using the same constant ignition rate for calculating new fire events. Ten year (2001 to 2010) simulations

were conducted for each threshold following the protocol of Rabin et al. (2017) (details in section 2.4). The results were fit against a data set of the frequency and duration of Canadian fires collected from 2001 to 2011 (Wang et al., 2014). An  $f_{\text{ext}}$  value of 1 new fire per day produced the best match to the data (Figure S1 in the supporting information) and was selected as the default value for this scheme.

### 2.3. Parameter Optimization

FINAL contains multiple tunable parameters that are optimized with respect to observed fire area burned using the same approach as in Rabin et al. (2017). In this scheme, the full terrestrial model is run for the 20 years from 1990 to 2009 (with meteorological forcing specific for those years) for 246 randomly selected grid points. The area burned for each point is optimized to the natural fire area burned from the GFED3s (Rabin et al., 2015; Randerson et al., 2012) on a monthly average basis for the years 2001–2009.

Previously, the tunable parameters were optimized to single, globally representative values (e.g., Rabin et al., 2017). Global area burned is dominated by tropical savanna and grassland fires, leading to an optimization that is tailored to tropical fires and may not be appropriate for fires in boreal and temperate zones that exhibit different ecosystem characteristics and fire activity (Archibald et al., 2013). Here we sort the 246 selected grid points into boreal and nonboreal subsets and optimize the parameters separately for each. Locations are characterized as boreal or nonboreal based on their Köppen climate zone classification (Köppen, 1936; Peel et al., 2007), with “cold” and “polar” climate zones comprising the boreal category. The cold and polar zones contain Canada, much of the northern United States, Russia, Scandinavia, northeastern China, and the Tibetan plateau. We use the Köppen climate zone data set from Kottek et al. (2006) who base their analysis on climate data from 1951 to 2000. Fifty-seven of the 246 grid points used for optimization were located in the boreal category, and the remaining 189 grid points were nonboreal.

Parameters that describe the fuel moisture, relative humidity, fuel availability, and anthropogenic ignitions and suppression functions were optimized using the optimized parameter values from FINAL.1 for initial values. We do not retune the ROS parameters for tropical biomes as in Rabin et al. (2017) since these are already specific to the tropics.

### 2.4. Experiment Setup

We label the version of FINAL that includes multiday burning, enhanced ROS in crown fires, and the separate optimization for boreal zones, as FINAL version 2 (FINAL.2), and compare its performance to the previous iteration, which we label in this study as FINAL.1 (Rabin et al., 2017). To make this comparison, we use the same initial setup of LM3 as in Rabin et al. (2017) in a series of present-day simulations run for 10 years between 2001 and 2010. All LM3 experiments are carried out at 2.5° longitude by 2.0° latitude horizontal resolution. Most LM3 processes are computed on a 30 min time step, including calculation of burned area and fire intensity. Fire emissions, fire-caused tree mortality, and multiday burning are computed on a daily time step. This configuration of LM3 includes the Carbon, Organisms, Rhizosphere, and Protection in the Soil Environment model (CORPSE; Sulman et al., 2014) that simulates production and decomposition of leaf litter and coarse wood litter carbon pools. LM3 was forced with time-varying atmospheric data from the Sheffield et al. (2006) data set that includes shortwave and long-wave radiation fluxes at the surface, precipitation, temperature, air pressure, specific humidity, and wind speed and direction. In addition, land use transitions follow the historical time series of Hurtt et al. (2011) that was used as forcing for Coupled Model Intercomparison Project phase 5 (CMIP5) simulations. Climatological monthly mean lightning flash density is sourced from the 1996–2014 Lightning Imaging Sensor (LIS) and Optical Transient Detector (OTD) low-resolution monthly time series product (Cecil et al., 2014), which was prepared as a climatology by Rabin et al. (2017). Human population data are from History Database of the Global Environment (HYDE) 3.1 (Klein Goldewijk et al., 2010) and interpolated linearly in time between data points to give annual populations. Initial conditions from Rabin et al. (2017) for year 2001 are used for this set of simulations. Note that using initial conditions developed with a FINAL.2 spin-up would lead to different results for this set of simulations, although the differences are likely to be superficial. In general, output for years 2002 to 2009 are used for analysis.

The set of present-day simulations includes (1) FINAL.1 (Rabin et al., 2017), (2) FINAL.1 with separate tropical and boreal optimized parameters (section 2.3), (3) FINAL.2 ( $f_{\text{ext}} = 0.5 \text{ fire day}^{-1}$ ), (4) FINAL.2 (default;  $f_{\text{ext}} = 1 \text{ fire day}^{-1}$ ), (5) FINAL.2 ( $f_{\text{ext}} = 3 \text{ fire day}^{-1}$ ), and (6) FINAL.2 ( $f_{\text{ext}} = 5 \text{ fire day}^{-1}$ ). Tunable parameters are optimized for each model setup for simulations (2) through (6).

**Table 1**  
*Details of the Data Sets Used to Drive the Set of Historical Simulations (1700–2010) Described in Section 2.4*

Simulation name	Lightning	Population	Land use	Fire effects
CTL	Pfeiffer et al. (2013)	HYDE 3.1	Hurt et al. (2011)	On
EXP1	Pfeiffer et al. (2013)	HYDE 3.1	Natural land cover	On
EXP2	Pfeiffer et al. (2013)	HYDE 3.1	Hurt et al. (2011)	Off
EXP3	Pfeiffer et al. (2013)	Constant year 1700	Hurt et al. (2011)	On
EXP4	LIS/OTD climatology	HYDE 3.1	Hurt et al. (2011)	On

The optimized FINAL.2 is then applied in a set of simulations covering the historical time period from 1700 to 2010. The basic LM3 framework remains the same as in the present-day simulations with the differences being in how transient input data sets is applied. A potential vegetation spin-up is used to provide the initial year 1700 conditions for these simulations. Here we define potential vegetation as the model state with solely natural land cover and no land use transitions applied. The spin-up is run for 300 years with preindustrial CO<sub>2</sub> concentration of 283 ppmv (representative of the year 1800). The Sheffield et al. (2006) atmospheric forcing from 1948 to 1972 is repeatedly cycled for all 300 years. Lightning input for these simulations is from a data set based on a climatology of the World-Wide Lightning Location Network (Virts et al., 2013) that has been extended by Pfeiffer et al. (2013) to cover the time period 1901 to 2013 using convection available potential energy (CAPE) fields from the Twentieth Century Reanalysis project (Compo et al., 2011). Lightning flash density data for 1948 to 1972 are continuously cycled throughout the potential vegetation spin-up to match the other atmospheric forcing. Three hundred years of simulation is sufficient to bring the above ground biomass carbon pools and fluxes into quasi-equilibrium. During the last 50 years of spin-up the global total fire area burned is  $5.0 \times 10^6$  km<sup>2</sup>, with global emissions of 3.0 Pg C yr<sup>-1</sup>. We run a separate 300 years of potential vegetation spin-up with no impacts of fires on the carbon cycle of LM3 to produce initial conditions for a historical transient run without fires.

Beginning in the initial year of the historical transient simulations, year 1700, with the initial conditions from the potential vegetation spin-ups, Hurtt et al. (2011) annual land use transitions are applied and human population increases following the HYDE 3.1 data set. Sheffield et al. (2006) atmospheric forcing from 1948 to 1972 continues to be cycled until year 1948 when the forcing year is arranged to correspond to the model year. Lightning forcing works similarly, cycling years 1948 to 1972 until the year 1948 when corresponding years are used for the remainder of the historical simulations. Global CO<sub>2</sub> concentration remains at preindustrial values (283 ppmv) for 1700 to 1800 and begins to increase in year 1800 following the historical trajectory. The historical simulations are run from year 1700 to 2010, and we test the sensitivity of trends and variability in fire emissions to various drivers by switching off, in turn, transient population, land use, interannually varying lightning, and fire carbon cycle impacts. Details of this set of five simulations are given in Table 1. For the analysis of the historical simulations we do not include fire emissions from burned coarse woody debris on grasslands, including all agricultural lands, noting that CORPSE is currently not configured to treat the decomposition of this litter pool properly for this land cover type. This is solely a diagnostic adjustment since coarse woody debris does not contribute to the aboveground carbon total that impacts fire spread rate.

Klein Goldewijk et al. (2017) describe an updated land use transitions data set, HYDE3.2, that includes improved representation of rice agriculture and grazing statistics based on more recent census data and a better understanding of time-varying per capita land use rates. Importantly for our assessment of FINAL.2, HYDE3.2 contains substantially larger areas of crop and pasture land globally than in HYDE3.1, which we are using for this study. Global cropland area in HYDE3.2 exceeds that of HYDE3.1 by nearly  $1 \times 10^6$  km<sup>2</sup> in the year 1800, and year 1800 pasture area is doubled in HYDE3.2 compared to HYDE3.1 (Klein Goldewijk et al., 2017). Yet midnineteenth century agricultural lands in HYDE3.2 are 40% lower than that reported in the alternative prehistorical land use time series developed by Kaplan et al. (2012). Since crop and pasture fire area burned is directly proportional to crop and pasture area in FINAL.2, the use of either of these higher land use data sets to drive fires in our simulations would add substantial amounts of area burned to our global totals during the 1700s and 1800s.

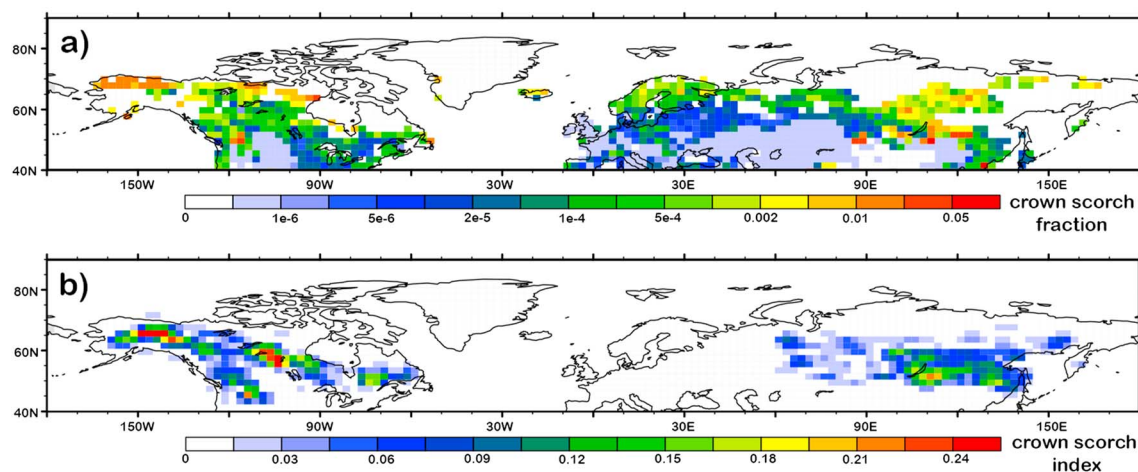


**Figure 1.** Representations of crown fire activity in boreal latitudes from (a) LM3, the annual average crown scorch fraction (unitless) from the present-day simulations (2002 to 2009), and (b) the crown scorch index from Rogers et al. (2015) (unitless) computed from data collected during 2003 to 2012.

### 3. Results

#### 3.1. Model Evaluation

In the present-day simulations, FINAL.2 predicts extensive areas of crown scorch in the boreal forests, particularly in the Canadian Rocky Mountain region and in southern Siberia (Figure 1). Assessment of this aspect of the model performance is difficult given the lack of regional-scale crown fire data available. Rogers et al. (2015) developed a crown scorch index that incorporates observations of fire radiative power, postfire albedo, and tree cover change. While not the same quantity produced by FINAL.2 (crown scorch fraction), the crown scorch index illustrates where crown fires are likely to be most frequent and important in boreal forests. Spatial comparison of the crown scorch fraction to the Rogers et al. (2015) index (Figure 1) largely validates the areas of maximum crown fire activity predicted by FINAL.2 in southern Siberia and northern Canada/Alaska. However, the modeled crown fires in northern Europe and Scandinavia are not evident in the observation-based scorch index (Figure 1). This could be a result of extensive forest management in the Scandinavian countries that reduces the potential for large, intense fires (Stocks et al., 2001), a process not represented in FINAL.2. The model is also not able to capture the difference in crown fire activity between North American and Eurasian boreal forests. Rogers et al. (2015) show that this intercontinental distinction is a result of differing tree species composition, another aspect not currently accounted for in LM3.

The Rogers et al. (2015) crown scorch index and other evidence (e.g., Wooster & Zhang, 2004) have established that crown fires are more common in North America than in Asia. However, the satellite-retrieved forest cover data introduced by Hansen et al. (2013) has been used to show that stand-replacing fires do occur frequently in Russia and exhibit seasonal and interannual variability (Krylov et al., 2014). As a proxy for crown fires, stand-replacing fires are biased high since surface fires also lead to extensive vegetation die-off, although with less frequency (Krylov et al., 2014). In a qualitative comparison, FINAL.2 is able to reproduce the annual time series of crown fire fraction reported by Krylov et al. (2014) between 2003 and 2008 with peaks in 2005 and 2007 (Figure S2). The model performs poorly in representing the seasonal cycle of the stand-replacing fire fraction (Figure S2) which is observed to peak in late summer, and the latitudinal distribution of the stand-replacing fire fraction (Figure S2) which is greatest between 60°N and 64°N (Krylov et al., 2014). In general, of the total natural burned area (i.e., excluding cropland and pasture fires) produced by FINAL.2 in Russia, roughly 2% to 4% is the result of crown fires (Figure S2). These estimates compare low to a previous estimate of crown fire fraction in this region of 16% to 24% (Gromtsev, 2002). This suggests that FINAL.2 is not fully capturing the enhanced fire ROS in boreal fires that spread to the crown.

Multiday burning in the FINAL.2 present-day simulations is important in the boreal regions but is more extensive in the tropics where extinguishing events are less common during the lengthy dry season (Figure 2). As a fraction of the total, multiday burned area is similar for tropical and boreal fires and generally ranges from 15% to 20%. For boreal fires, the percentage of area burned by multiday burning in FINAL.2 is probably an



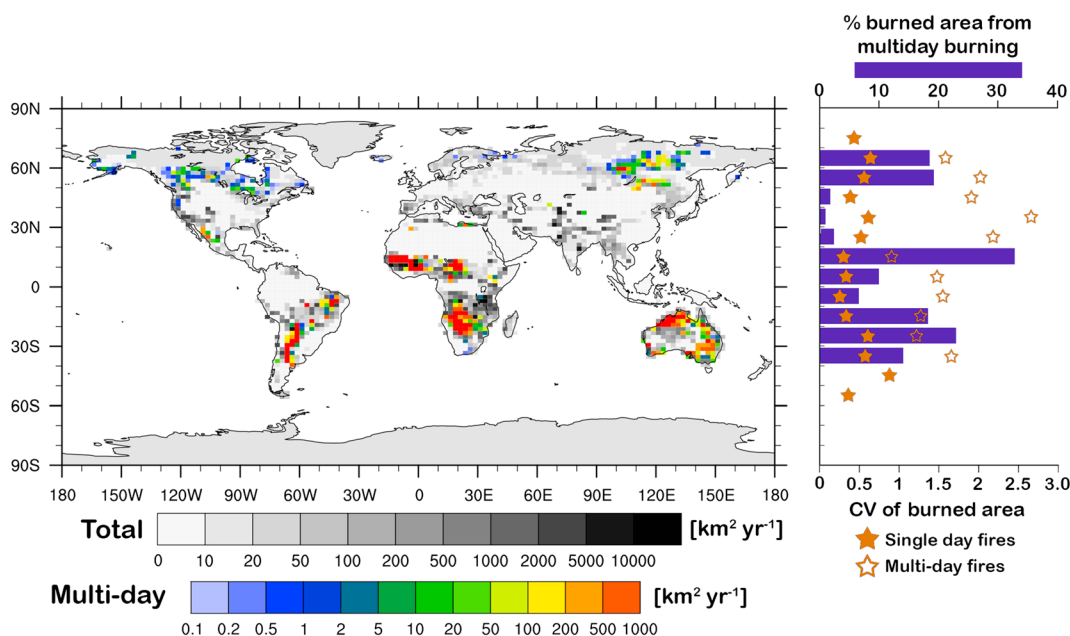


**Figure 2.** The spatial distribution of annual average burned area from wildfires (fires on natural or secondary lands) from the present-day LM3 simulations with all wildfires in black and white and multiday burning burned area only in colors. The latitude band average fraction of burned area from multiday burning is shown in the bar graph with the coefficient of variation represented by the stars for single-day burning (closed stars) and multiday burning (open stars).

underestimate. Characterizations of observed boreal fire frequency and size suggest that the vast majority of area burned (>90%) results from the small number of very large fires (<5%) that escape management and burn for multiple days (e.g., Stocks et al., 2002). Since FINAL.2 is able to reproduce the distribution of fire frequency against duration for boreal Canadian fires (Figure S1), we conclude that the model underpredicts the burned area per fire for long duration events. This could result from coarse grid-averaged wind forcing that does not include local high wind events (e.g., Lasslop et al., 2015), imposed maximum ROS, or assuming a single ignition point for individual fires. The 30 day limit on fire duration that we impose eliminates the potential for simulating the longest observed events, but with the current model setup, boreal fire duration in FINAL.2 rarely exceeds even 20 days. The 2016 Fort McMurray fire in Alberta, Canada, consumed over 700 km<sup>2</sup> in a single day during its 40 day duration (Alberta Agriculture and Forestry, 2017), whereas the FINAL.2 fire daily area burned for the boreal region between 2003 to 2009 reaches a rate of 30 km<sup>2</sup> d<sup>-1</sup> about twice a year, with six 100 km<sup>2</sup> d<sup>-1</sup> events in this time period, four taking place during 1 year in North America.

The multiday fire burned area in FINAL.2 relies on uninterrupted periods of dry conditions and these are variable on a year-to-year basis. At all latitudes, the IAV of multiday fire burned area, represented here by the coefficient of variation of annual totals (2003–2009), far exceeds the IAV of single day fires (Figure 2). In this way, the introduction of multiday burning acts to increase the IAV of global fire area burned.

### 3.2. Validation of FINAL.2

Optimizing the tunable parameters within FINAL.2 separately for boreal and nonboreal locations results in different parameter values compared to the global optimization (Figure 3). With the new parameter set, both boreal and nonboreal fires are responsive to changes in relative humidity. This makes relative humidity especially important as an extinguishing factor for multiday burning since it exhibits a diurnal cycle, typically increasing at night. Also in both regions, particularly for boreal fires, burning will occur for higher values of the soil moisture factor,  $\theta$ , compared to FINAL.1. For FINAL.2, the impact of above ground biomass on fire events remains roughly the same as for FINAL.1 in the tropics, but a much larger amount of biomass is required to support burning for boreal fires. This could be a result of the optimization routine effectively scaling down the boreal fire burned area that has been increased by enhanced ROS in crown fires and multiday

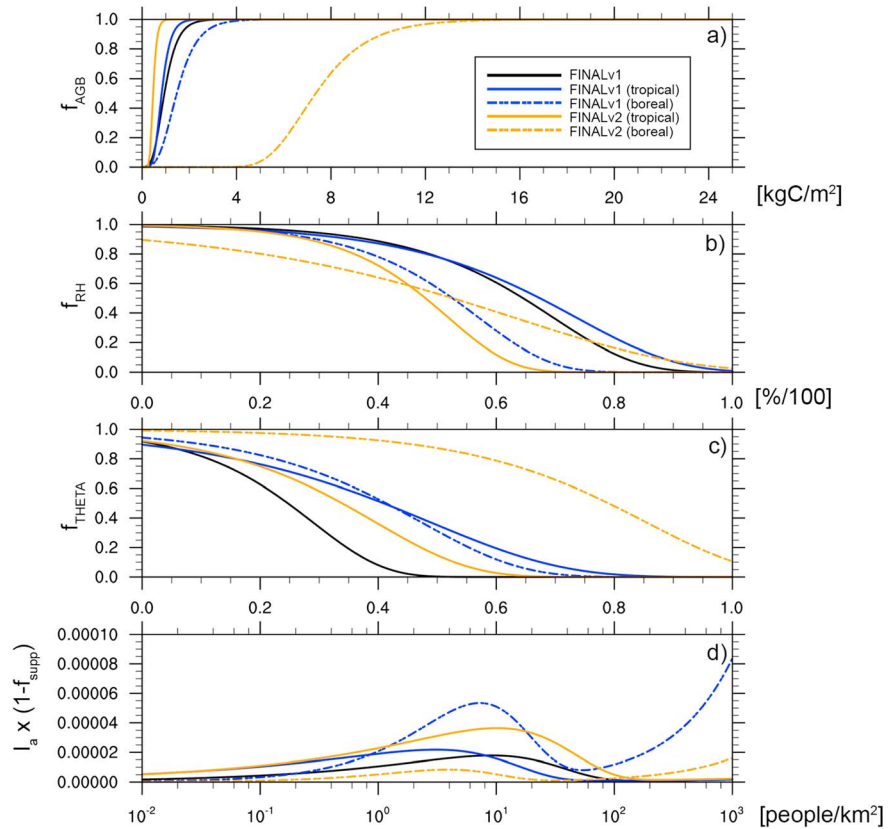


**Figure 3.** Fraction of ignitions becoming fires as a function of (a) aboveground biomass, (b) relative humidity, and (c) soil moisture, and (d) the number of ignitions as a function of human population for FINAL.1 (black line), FINAL.1 nonboreal (blue, solid line), FINAL.1 boreal (blue, dashed line), FINAL.2 nonboreal (orange, solid line), and FINAL.2 (orange, dashed line).

burning. In the tropics it appears that a similar scaling effect was accomplished by adjusting the moisture-related functions, relative humidity, and  $\theta$  (Figure 3).

To assess the relative performance of the two versions of the fire model, we compare the results from the present-day simulations to burned fraction and carbon emissions data from the GFED with small fires (Randerson et al., 2012) version 4 (GFED4s) for 2002–2009. Including the new optimized parameters and the multiday fire and crown fire schemes in FINAL.2 leads to improvement in representation of boreal burned fraction (Figure 4). These fires were missing in large part from FINAL.1, and while FINAL.2 shows a substantial increase in this quantity compared to the previous model version (Figure 4d), it still underpredicts boreal fire area burned in general (Figure 4e).

FINAL.2 burned fraction is decreased in equatorial regions, especially in Africa (Figure 4), where the high relative humidity is now a limiting factor for fires. Outside of the tropics, FINAL.2 generally simulates increased fires compared to FINAL.1. This results from a combination of greater anthropogenic ignition rates (Figure 3d) and the sustaining of multiday burning in areas with moderately moist soils (theta between 0.4 and 0.6) that do not support wildfires in FINAL.1. FINAL.2 results correlate better spatially with the GFED4s ( $r^2 = 0.68$ ; log-transformed burned area data) than the FINAL.1 results ( $r^2 = 0.40$ ), and the global annual burned fraction for FINAL.2 (431 Mha) is closer to GFED4s (467 Mha) compared to FINAL.1 (406 Mha).

The spatial correlation between the global annual carbon emissions from fires in FINAL.2 and the same quantity in GFED4s ( $r^2 = 0.66$ ) also shows improvement (FINAL.1  $r^2 = 0.57$ ) (Table 2). Overall, the differences between FINAL.1 and FINAL.2 follow that of the burned area with increased boreal emissions in the new version and a patchwork of increases and decreases in the tropics and temperate latitudes (Figure 5). Emissions from fires are underpredicted compared to GFED4s in the tropics, especially in areas closest to the equator. In

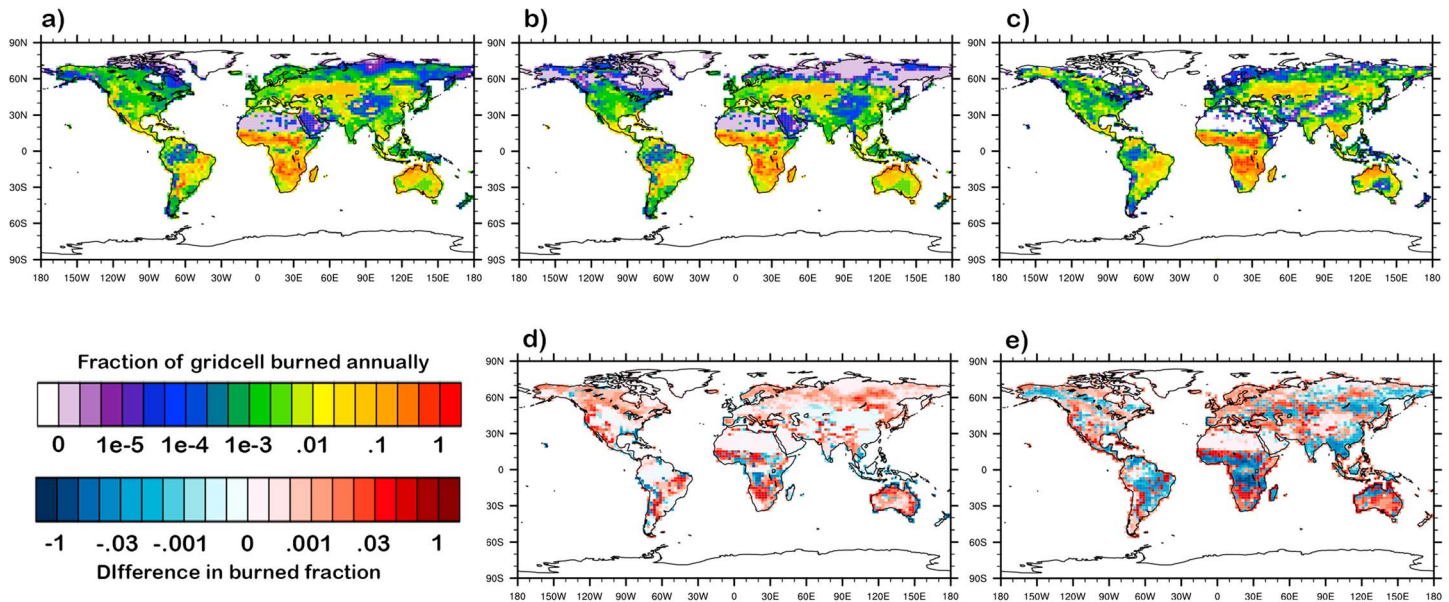


**Figure 4.** The spatial distribution of annual average burned fraction from all fires for (a) FINAL.2, (b) FINAL.1, (c) GFED4s, averaged over years 2003–2009, (d) the difference between FINAL.2 and FINAL.1 and (e) the difference between FINAL.2 and GFED4s.

FINAL.2, boreal emissions are high on average relative to GFED4s, even though the burned area is similar. This could result from different fuel load or combustion completeness in LM3 compared to the model used to produce carbon emission estimates in GFED4s and the different spatial distributions of the burned area within the boreal region in FINAL.2 and GFED4s. For example, FINAL.2 overpredicts burned area in high-carbon content areas including Scandinavia and northern Canada, leading to an even greater overprediction of carbon emissions.

FINAL.2 results also show improved correlation with the time series of carbon emissions from GFED4s for the years 2002 to 2009 (Figure 6; Table 2), while the time series of global area burned for FINAL.2 and FINAL.1 are nearly identical (Figure S3). In FINAL.1, fire emissions in the Northern Hemisphere winter are large compared

**Table 2**

*Fire Carbon Emissions Statistics From Years 2002–2009 of the Present-Day Simulations Using FINAL.1 and FINAL.2 Compared to the Values for GFED4s From the Same Time Period*

Region	Annual mean (Tg C)			Coefficient of variation			Temporal correlation coefficient		Spatial correlation coefficient	
	FINAL.1	FINAL.2	GFED4s	FINAL.1	FINAL.2	GFED4s	FINAL.1	FINAL.2	FINAL.1	FINAL.2
BONA	17	121	71	0.58	0.50	0.43	0.06	0.48	0.06	0.29
TENA	56	34	16	0.46	0.21	0.37	0.50	0.62	0.06	0.37
CEAM	51	41	23	0.30	0.22	0.56	0.75	0.57	0.62	0.69
NHSA	40	29	28	0.23	0.17	0.48	0.49	0.76	0.27	0.36
SHSA	339	389	284	0.28	0.21	0.50	0.46	0.82	0.51	0.68
EURO	21	22	5	0.22	0.05	0.22	0.42	0.80	0.38	0.26
MIDE	10	22	1	0.39	0.32	0.23	0.31	0.74	0.33	0.35
NHAF	547	406	428	0.10	0.08	0.06	0.63	0.91	0.79	0.78
SHAF	742	608	668	0.12	0.13	0.04	0.75	0.94	0.76	0.79
BOAS	23	164	133	0.10	0.27	0.70	0.44	0.51	0.41	0.47
CEAS	159	144	70	0.51	0.22	0.12	0.69	0.60	0.55	0.64
SEAS	134	55	104	0.29	0.16	0.32	0.22	0.78	0.30	0.59
EQAS	14	7	97	0.12	0.15	0.80	0.47	0.65	0.44	0.37
AUST	85	200	95	0.21	0.22	0.46	0.77	0.62	0.69	0.69
GLOBAL	2236	2272	2021	0.07	0.09	0.09	0.40	0.86	0.57	0.66

Note. Correlation coefficients are computed between the fire model indicated and the GFED4s data set.

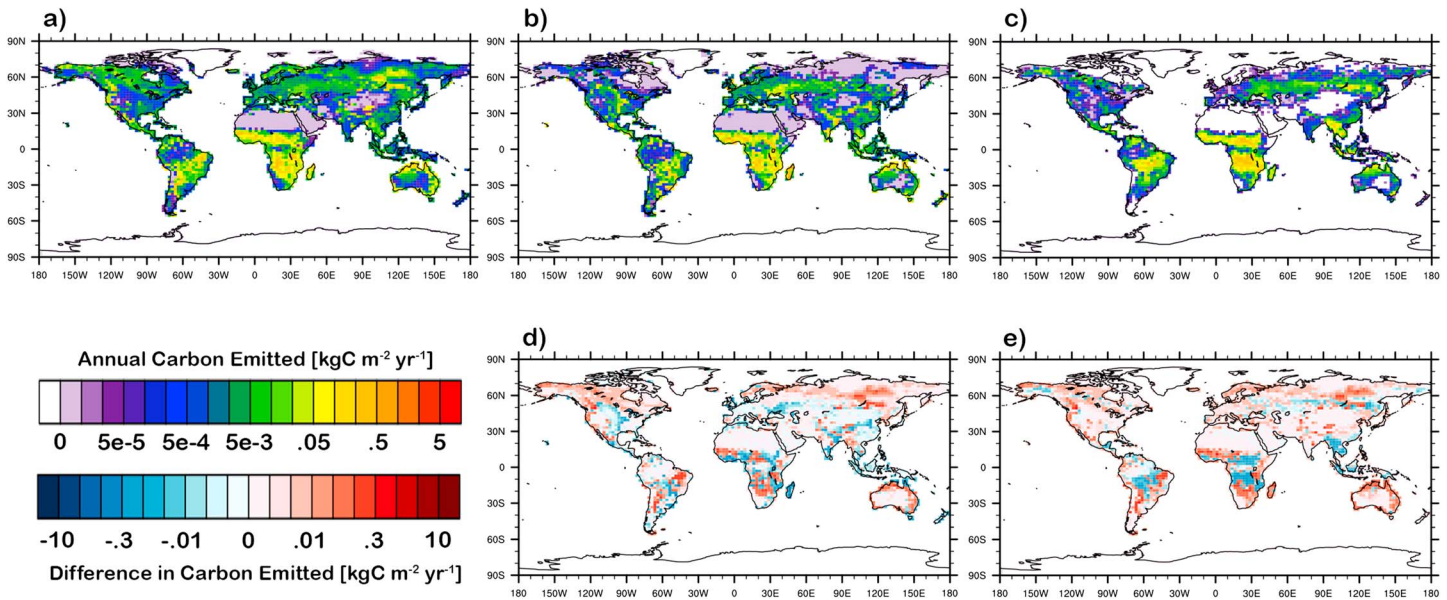


**Figure 5.** The spatial distribution of annual average carbon emissions from all fires for (a) FINAL.2, (b) FINAL.1, (c) GFED4s, averaged over years 2003–2009, (d) the difference between FINAL.2 and FINAL.1, and (e) the difference between FINAL.2 and GFED4s.

to GFED4s, especially in North Africa and Central America, altering the seasonality of the global emissions. The Fire Inventory (FINNV1.5; Wiedinmyer et al., 2011) and the Global Fire Assimilation System (GFASv1; Kaiser et al., 2012) data sets are derived from an active fire product that captures small fires emissions more effectively than the area burned-based GFED4s. Emissions from small fires are especially important in Central America and Southeast Asia where agricultural waste burning is prevalent (Andela et al., 2013). Southeast Asia emissions are particularly high in FINNV1.5, contributing to the February/March maxima in global emissions shown for this inventory in Figure 6. FINAL.2 does not capture these maxima but does match well with FINNV1.5 estimates of Central America fire emissions. Both versions of FINAL overestimate temperate North America emissions with respect to GFED4s (Table 2) but are a better match with GFASv1, which reports more extreme fire seasons in that region than FINNV1.5 or GFED4s. There is sufficient disagreement among the different satellite product-based fire emissions inventories that the annual cycle of fire emissions from both FINAL.2 and FINAL.1 lie within the inventory range (Giglio et al., 2013; Kaiser et al., 2012; Wiedinmyer et al., 2011). However, FINAL.2 correlates better with the GFED inventory that is used for optimization in both cases. Changes in the interannual variability of boreal fire emissions between FINAL.1 and FINAL.2 are not apparent from the global totals shown in Figure 6 which are dominated by tropical fires.

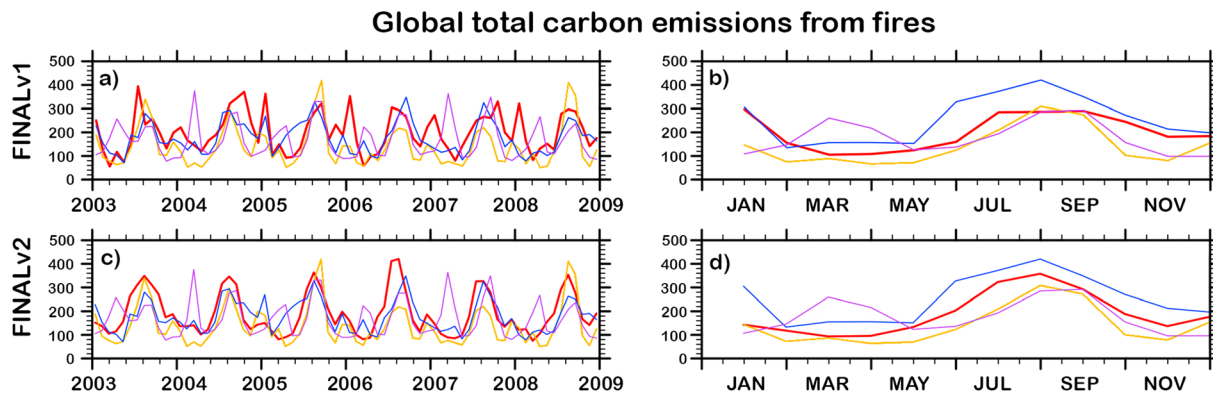


**Figure 6.** Timeseries of carbon emissions from fires ( $\text{Tg C month}^{-2}$ ) output from the present-day set of simulations for (a) 2003 to 2009 from FINAL.1, (b) annual cycle (averaged over 2003 to 2009) from FINAL.1, (c) 2003 to 2009 from FINAL.2, and (d) annual cycle (averaged over 2003 to 2009) from FINAL.2 compared to data from GFED4s (yellow lines), GFASv1 (blue lines), and FINNV1.5 (purple lines).

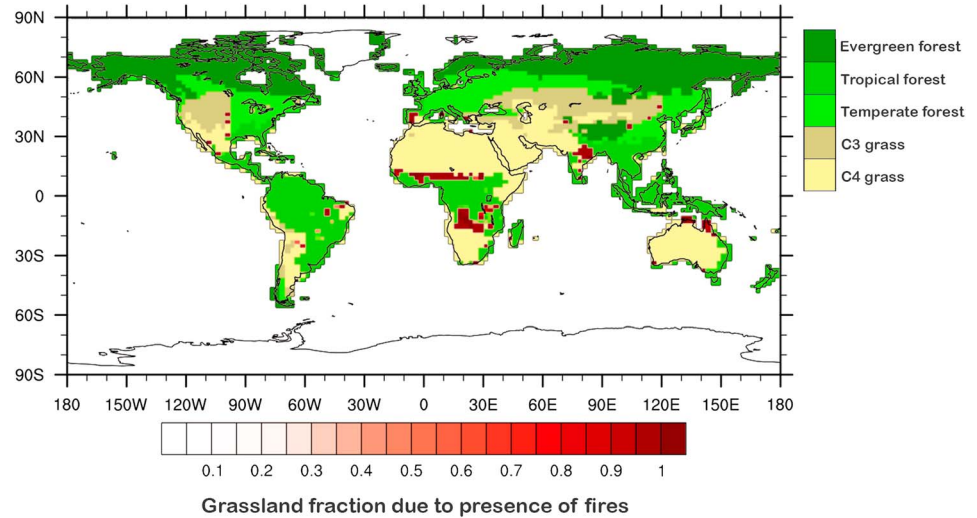


**Figure 7.** The difference in fractional area of grassland between the FINAL2 spin-up simulations with and without fires superimposed onto the distribution of vegetation species at the end of the spin-up simulation.

### 3.3. Historical Impacts of Fires on Carbon Cycle

After the 300 year spin-up of LM3 with potential vegetation, the presence of fires has altered the spatial distribution of vegetation, particularly in the tropics. Fires cause the expansion and maintenance of grassland ecosystems in LM3 in parts of central Africa, northern Australia and India (Figure 7), an effect also noted in the nineteenth century in Africa (Brönnimann et al., 2009). The spatial distribution of grasses replacing forest in the tropics closely resembles the pattern shown in Bond et al. (2004), which demonstrated that “switching off” fires in a dynamic global vegetation model affects forest-grass boundaries, although that study was using a fairly simple representation of fire occurrence and fire C flux. A more recent study shows that multiple stable ecosystem states can be achieved with some models in tropical regions due to feedbacks between fires and fractional tree cover (Lasslop et al., 2016). Bond et al. (2004) also found a reduction of extratropical forest area by fires in their simulations, especially in Europe, and also noted that species composition may be dramatically altered by fires in boreal forests even if the region remains forested.

In FINAL2, midlatitude and boreal fires are not frequent enough to maintain levels of biomass below the LM3-defined threshold for the forest biome, except in a few isolated locations, including some along the European Mediterranean coast (Figure 7). Improved accounting of crown fires and their effects on vegetation could lead to a different equilibrium state in boreal forests, possibly with reduced forest area.

In addition to perpetuating grasslands in the tropics, fires also maintain lower carbon storage in forests by stunting vegetation growth and by removing dead biomass carbon, such as leaf litter and coarse woody debris, from the terrestrial biosphere, while net primary production remains similar with or without fires (Figure 8) (Yue et al., 2015). Model results show that these maintenance effects could lead to an atmospheric CO<sub>2</sub> concentration that is 40 ppm higher compared to a world without fires (Ward et al., 2012). In FINAL2, fires reduce the living biomass carbon by about 100 Pg C after the potential vegetation spin-up, with this difference decreasing to about 50 Pg C during the twentieth century (Figure 8), an indication that the carbon flux from the biosphere to the atmosphere from all types of disturbance, mainly LULCC, is decreased when fires are included. Fires reduce the amount of carbon available to be released to the atmosphere or into litter and

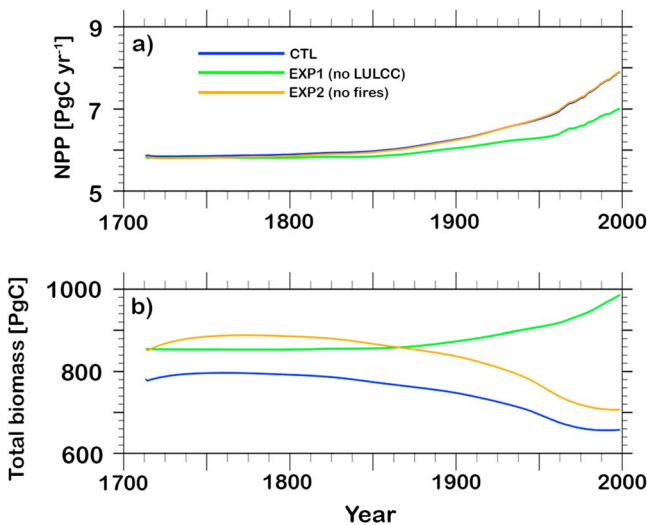


**Figure 8.** Twenty-five year running average time series of (a) net primary productivity (NPP) ( $\text{Pg C yr}^{-1}$ ) and (b) total living biomass ( $\text{Pg C}$ ) from 1700 to 2010 for the CTL (blue), EXP1 with no LULCC (green) and EXP2 with no fires (orange).

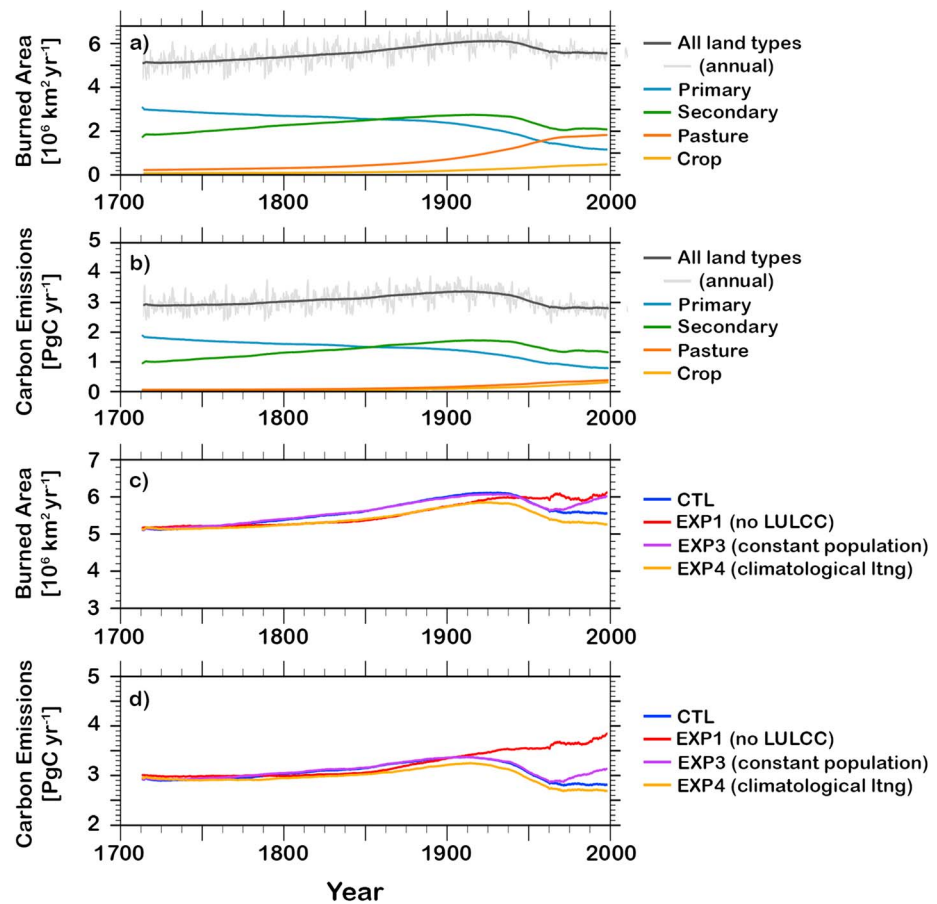


**Figure 9.** Time series from 1700 to 2010 of (a) burned area and (b) carbon emissions for all fires annual average (gray) and 25 year running average (black), and for natural land type (blue), secondary land type (green), pasture (orange), and cropland (yellow), all 25 year running average. Time series from 1800 to 2010 of (c) burned area and (d) carbon emissions for experiments CTL (blue), EXP1 (no LULCC) (red), EXP3 (constant population) (orange), and EXP4 (climatological litng) (purple).

product pools following deforestation or vegetation harvesting. This effect was also shown by Ward and Mahowald (2015), which attributed about half of this carbon flux reduction to lower LULCC carbon emissions and half to LULCC-driven reductions in fire activity.

The carbon flux to the atmosphere from fires in FINAL2 increases from  $3.0 \text{ Pg C yr}^{-1}$  in 1700 to  $3.3 \text{ Pg C yr}^{-1}$  by the year 1900, peaks at  $3.4 \text{ Pg C yr}^{-1}$  in the year 1920 and then begins to decline in recent decades (Figure 9b). The late twentieth century decrease reflects a transition from fires burning mostly natural and secondary lands to fires burning more area on agricultural lands that on a global basis contain less biomass and emit less carbon (Figures 9a and 9b). The historical trend in fire emissions shown here agrees with the model results of Pechony and Shindell (2010) (who report fire counts instead of emissions), Kloster et al. (2010), and Ward et al. (2012). The latter two studies use an earlier version of the Li et al. (2012, 2013) model that was the basis for FINAL. Reconstruction of global fire activity using charcoal sediment data suggests that fires peaked in year 1870 before beginning to decline (Marlon et al., 2008). Uncertainties remain with regard to age estimation of charcoal samples and in estimating emissions from the accumulation rates, which are affected by many natural processes (Marlon et al., 2016), but on a global scale this proxy can be used to indicate long-term trends. A more recent analysis of an expanded, global charcoal sediment data set shows a secondary maximum of global fire emissions in the midtwentieth century (Marlon et al., 2016), similar in a qualitative sense to the FINAL2 historical time series. van Marle et al. (2017) developed a fire emissions data set that will be used to drive CMIP6 models by combining satellite retrievals with proxy records and model results. Their time series shows relatively constant global fire emissions between the years 1750 and 2010 with a small decline after the 1990s. Other historical data sets that report burned area as a measure of fire

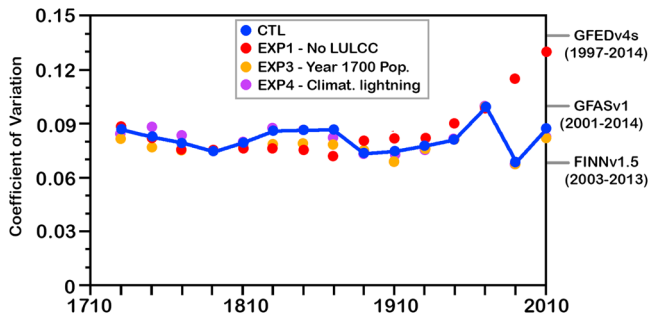


**Figure 10.** Coefficient of variation of global, annual fire emissions calculated for 20 year segments and plotted at the ending of every segment. The values for the different experiments are compared to values from present-day inventories (FINNv1.5; Wiedinmyer et al., 2011; GFASv1; Kaiser et al., 2012). Note the value for the GFED4s is different than the value given in Table 2 because here we compute the variability over a different time period (1997 to 2014).

activity show an increase between 1900 and today (e.g., Mieville et al., 2010; Mouillot & Field, 2005). In contrast to FINAL2, recent satellite analysis of area burned shows a steep decline (24%) over the past 18 years (Andela et al., 2017) as a result of expanded land use.

### 3.4. Impacts of Population/LULCC on Global Fire Trends and Variability

Changes in human population between 1800 and 2010 drive global fire emissions downward, with almost all of this decrease realized since 1970 (Figure 9d). Population growth leads to increased fire events in FINAL2 due to additional fire ignitions until population density exceeds about 5–10 people per square kilometer (Figure 3). At the higher population density, suppression of fires becomes the dominant effect. Population densities in the year 2010 for boreal forests do not exceed 10 people per square kilometer in most locations, but in tropical and subtropical regions that are prone to fires, these higher population

densities are common. As human population rapidly increased in the tropics and subtropics during the latter half of the twentieth century, the suppressive effect of people became large enough to decrease fire emissions by about 10% (Figure 9d). Previous modeling efforts have shown a near-neutral contribution (Kloster et al., 2010), a large positive contribution peaking midcentury (Pechony & Shindell, 2010), and a small negative contribution (Knorr et al., 2016; Yang et al., 2014) of population growth to the twentieth century fire trend. Much of the disagreement stems from differences in the parameterization of the population impact on fire suppression between models. On a global scale, our results are consistent with the analyses of Bistinas et al. (2014) and Knorr et al. (2014) who showed using observational data sets that the principal effect of population on fires is suppression, whereas additional ignition by people is a relatively minor effect.

The effect of historical LULCC has also been to decrease global fire activity, but with both a larger and longer-term impact than human population growth (Figure 9). The replacement of natural land fires with lower biomass agricultural land fires, especially in the tropics, reduces global fire emissions by about 30% by the year 2010 in FINAL2. Earlier modeling studies (i.e., Kloster et al., 2010; Pechony & Shindell, 2010) show reductions in global fire emissions due to historical LULCC of between 5% and 20%, but more recent analysis suggests a larger role for LULCC (Andela et al., 2017). We expect that the use of a higher land use data set, such as HYDE3.2 (Klein Goldewijk et al., 2017) to drive land use transitions would lessen the gradual increase in fire emissions during the 1700s and 1800s shown in Figure 9. This could improve the comparison of our results with the historical emissions inventory produced by van Marle et al. (2017). Most global fire models are structured such that LULCC can decrease fires on natural lands indirectly by reducing the average aboveground biomass of the grid cell (Ward & Mahowald, 2015). Here because of the tiling framework of LM3, natural lands' aboveground biomass is not reduced by adjacent land cover changes within a grid box, thereby removing this potential artifact of averaging biomass for fire modeling on the coarse model resolution. Fire size in FINAL2 may still be reduced by fragmentation of the landscape, which is related to LULCC (Rabin et al., 2017).

Interannual variability of fire emissions, shown for 20 year segments in Figure 10, does not exhibit a trend in the historical period. We compute the coefficient of variation of the 20 year segments using only nonagricultural fire emissions. When a climatological annual cycle of lightning is used to drive fire ignition (EXP4) in place of the interannually varying data set, global fire emissions IAV is reduced, but the reduction is small. Recent observational evidence shows lightning can be a major driver of year-to-year variability in fire area burned in Alaska (Veraverbeke et al., 2017). However, FINAL2 shows little change in boreal North America fire emissions variability when using an annual lightning climatology (EXP4) compared to CTL, suggesting that FINAL2 is more responsive to variability in atmospheric and fuel moisture than lightning. A more realistic representation of fire ignition would include observed or modeled lightning strikes that are synchronous with the meteorology used to drive the land model (Felsberg et al., 2017) and could be used to explore the importance of lightning proposed by Veraverbeke et al. (2017). Differences in IAV caused by interannually varying lightning and population change are smaller than the range in IAV in the CTL during the 1800 to 2010 time period. In contrast, when LULCC is excluded, nonagricultural fires become much more variable from 1970 to

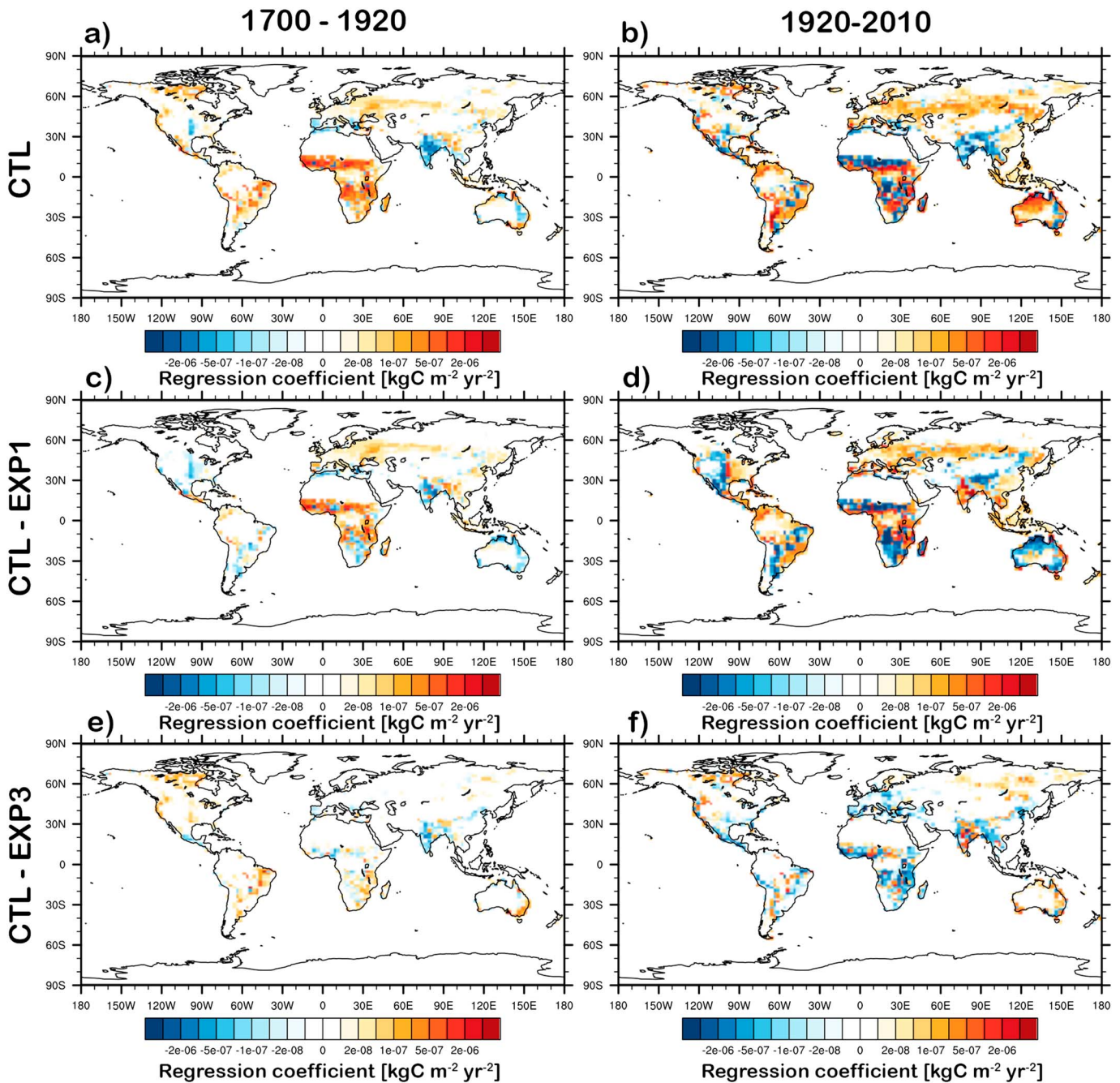


**Figure 11.** Linear regression coefficient of annual fire emissions ( $\text{kg C m}^{-2} \text{yr}^{-2}$ ) at each grid point for the CTL experiment (a) years 1700–1920, and (b) years 1920–2010, for the CTL experiment minus EXP1 (c) years 1700–1920, and (d) years 1920–2010, and for the CTL experiment minus EXP3 (e) years 1700–1920, and (f) years 1920–2010.

2010. This effect of land use on fire variability is evident in all major agricultural regions for the most recent 20 year segment (Figure S4b).

The separate representation of pasture and cropland fires in FINAL improves the seasonality of fires (Rabin et al., 2017) by accounting for the different timing of pasture and cropland burning, which is driven partially by human decision-making. However, the interannual variability of combined agricultural and nonagricultural fire area burned and emissions is reduced by our use of a single, averaged annual cycle for fractional area burned on crop and pasture lands. In general, agriculture and other land maintenance fires are more



consistent from year to year than wildfires (Giglio et al., 2013), but the areal extent of human-controlled fires is still dependent in part on the ambient conditions. In Indonesia, land-clearing fires are set on an annual basis but spread beyond the intended area during dry years or even short dry spells (Gaveau et al., 2014; Marlier et al., 2015). In all, FINAL2 fire IAV is artificially reduced by the use of a single annual cycle of fractional area burned for agricultural fires. Moreover, the crop and pasture fractional area burned data sets were developed for modern-day agricultural practices. Strategies and rules governing the use of fire in agriculture change over time. We recommend future development that accounts for these changes to produce a more representative historical simulation of agricultural fires.

### 3.5. Regional Trends in Historical Fire Activity

Trends in fire emissions are spatially heterogeneous and on a regional basis do not always conform to the global trend. Instead, different fire drivers dominate in different areas depending on the local land use, demographic, and climate changes. Between 1700 and 1920, fire emissions increase in nearly all regions (Figure 11a). In South Asia fire emissions decrease, which can be explained partly by LULCC that took place over this time period, without a large impact of population change (Figures 11c and 11e). Emissions increase over central Asia and Europe in response to LULCC. Much of the increase in fire emissions in tropical Africa and South America can likewise be attributed to LULCC between 1700 and 1920. After 1920 and through 2010, fires maintain trends from the previous time period across Eurasia, the Americas, and Australia, with minor exceptions in the eastern United States and parts of Europe (Figure 11b). However, major changes are evident in Africa where some areas continue to experience a high rate of increase in fire emissions, but fires have greatly decreased in adjacent grid points, containing mostly savanna and also some forests. These contrasting trends are driven largely by LULCC (Figure 11d), and it is the decreasing trends in Africa that drive the global mean fire emissions downward in the second half of the twentieth century. Figure 11 illustrates that global fire emissions would be much greater in present-day Africa without the human impacts on land cover, while South American fires would be greatly decreased. This is consistent with our understanding of the impacts of the conversion of tropical landscapes to croplands on fires, thought to have led to a global decrease in fires (e.g., Houghton et al., 1999), particularly in Africa (Andela & van der Werf, 2014) and South Asia (Yang et al., 2014), but with increases in fire activity in South America (e.g., Nepstad et al., 2006; Chen et al., 2013). The impact of changing population on fire emissions in the tropics is minor except for a few small areas where large human population change coincides with an active fire zone (Figure 11f). In contrast, population change is the major driver of increases in boreal fire emissions between 1920 and 2010 in the FINAL2 simulations.

## 4. Conclusions

FINAL2 combines an optimized version of the Li et al. (2012, 2013) fire model with fire intensity following Thonicke et al. (2010), multiday burning in the vein of Le Page et al. (2015), and the agricultural fire model from Rabin et al. (2017) to create a unique modeling system with reduced biases in boreal fires compared to FINAL1 and more accurate interannual variability in global fire emissions. In a study of historical fire IAV, we find that the variability of global fire area burned and emissions does not change substantially during the historical period in our simulations but is impacted by LULCC. Nonagricultural fires are less variable on an interannual basis during the latter half of the twentieth century due to LULCC.

Evidence from proxy records of past fire activity and written records suggest that global average emissions from fires have decreased during the twentieth century. We find that this decrease is tied closely to land use land cover changes, with the expansion of crop and pasture lands leading to increased area burned globally but fewer emissions, as carbon-dense forests are replaced with agricultural lands with lower biomass vegetation. Our results also show about a 10% reduction in present-day fire emissions from increases in human population, consistent with the work of Knorr et al. (2016) on fire suppression.

While the predictions of the fire model are improved, FINAL2 does contain limitations in its representation of global fire activity. Deforestation occurs as a land use land cover change in LM3, but the carbon removed during this process is sent to long-lifetime wood product and litter pools instead of being released immediately into the atmosphere by fire, as occurs in some regions. According to van der Werf et al. (2010), deforestation is the dominant fire type throughout much of the tropical forests and accounts for up to 25% of global fire emissions. Past modeling efforts put the percentage of global carbon emissions from deforestation fires between about 10% and 25% (Kloster et al., 2010; Li et al., 2013). If this source of carbon emissions, which

is most important beginning in the midtwentieth century, was included in FINAL2, we would expect to see a smaller late twentieth century decrease in global fire emissions or possibly an increasing trend during that time period. The burning of peat carbon is not included in FINAL2 (a peat fire scheme has been developed by Li et al., 2013 and used in other models). These smoldering fires are especially important in equatorial Asia, where draining of peatlands during land use has made the landscape more combustible and the fire emissions more variable from year to year. Fire emissions in equatorial Asia come almost entirely from deforestation, degradation, and peat burning (van der Werf et al., 2010). This explains, to a large degree, why FINAL2 under predicts fire emissions in this region (Table 2). Including representation of peat fires, along with deforestation and degradation fires, could lead to substantial improvement in the model simulation of global fires and fire emissions.

Altogether, we are now able to better simulate the spatial distribution and IAV of global fires within the GFDL modeling system. The ability of FINAL2 to better match the observed year-to-year variations in global fire emissions suggests that the response of the model to fluctuations in climate has been generally improved relative to previous studies. This lends confidence to FINAL2 for simulating future changes in fire activity related to a changing climate. Past modeling studies generally conclude that future climate change will lead to greater fire activity globally (e.g., Kloster et al., 2012). Our results suggest that these increases may be tempered by continuing land use and land cover changes, particularly tropical deforestation, similar to the conclusions of Andela et al. (2017). Standard outlooks of land use for driving models project a reduction in tropical deforestation, although these may underestimate present-day deforestation and be too optimistic about future rates of forest loss (Hansen et al., 2013; Mahowald et al., 2017).

Fires in the northern forests of Asia and North America are thought to be especially responsive to warming temperatures because temperature-dependent factors including warm season length and relative humidity are important predictors of fire activity in these regions (Flannigan et al., 2009). These fires may also depend considerably on changes in lightning activity (Veraverbeke et al., 2017). Here where the anthropogenic impact on land cover is small, trends and variability in fires are driven by the occurrence of extreme fires. Our updates to the existing global fire model improve representation of long-lived, fast-moving fires but appear to be too conservative to capture megafire events. Future development in this area with an aim toward improved simulation of the frequency-area distribution of fires could improve our confidence for modeling future changes in boreal fire activity.

#### Acknowledgments

This report was prepared by D. Ward under award NA14OAR4320106 from the National Oceanic and Atmospheric Administration (NOAA), U.S. Department of Commerce. The statements, findings, conclusions, and recommendations are those of the authors and do not necessarily reflect the views of NOAA, or the U.S. Department of Commerce. Model output data and the FINAL2 module used for this study are publicly available here: <https://doi.org/10.5281/zenodo.1098591>

#### References

- Abatzoglou, J. T., & Kolden, C. A. (2013). Relationships between climate and macroscale area burned in the western United States. *International Journal of Wildland Fire*, 22(7), 1003–1018. <https://doi.org/10.1071/WF13019>
- Adams, M. A. (2013). Mega-fires, tipping points and ecosystem services: Managing forests and woodlands in an uncertain future. *Forest Ecology and Management*, 294, 250–261. <https://doi.org/10.1016/j.foreco.2012.11.039>
- Alberta Agriculture and Forestry (2017). *A review of the 2016 Horse River fire* (p. 92). Edmonton, Canada: MNP LLP.
- Andela, N., Kaiser, J., Heil, A., van Leeuwen, T., van der Werf, G., Wooster, M., ... Schultz, M. (2013). Assessment of the Global Fire Assimilation System (GFASv1), MACC-II (Monitoring Atmospheric Composition and Climate) project. Retrieved from <http://juser.fz-juelich.de/record/186645> (last access: 15 December 2017)
- Andela, N., Morton, D. C., Giglio, L., Chen, Y., van der Werf, G. R., Kasibhatla, P. S., ... Randerson, J. T. (2017). A human-driven decline in global burned area. *Science*, 356(6345), 1356–1362. <https://doi.org/10.1126/science.aal4108>
- Andela, N., & van der Werf, G. R. (2014). Recent trends in African fires driven by cropland expansion and El Niño to La Niña transition. *Nature Climate Change*, 4(9), 791–795. <https://doi.org/10.1038/nclimate2313>
- Archibald, S., Lehmann, C. E. R., Gomez-Dans, J. L., & Bradstock, R. A. (2013). Defining pyromes and global syndromes of fire regimes. *Proceedings of the National Academy of Sciences*, 110(16), 6442–6447. <https://doi.org/10.1073/pnas.1211466110>
- Arora, V. K., & Boer, G. J. (2005). Fire as an interactive component of dynamic vegetation models. *Journal of Geophysical Research*, 110, G02008. <https://doi.org/10.1029/2005JG000042>
- Balch, J. K., Bradley, B. A., D'Antonio, C. M., & Gómez-Dans, J. (2013). Introduced annual grass increases regional fire activity across the arid western USA (1980–2009). *Global Change Biology*, 19(1), 173–183. <https://doi.org/10.1111/gcb.12046>
- Bistinas, I., Harrison, S. P., Prentice, I. C., & Pereira, J. M. C. (2014). Causal relationships vs. emergent patterns in the global controls of fire frequency. *Biogeosciences*, 11(3), 3865–3892. <https://doi.org/10.5194/bgd-11-3865-2014>
- Bistinas, I., Oom, D., Sá, A. C. L., Harrison, S. P., Prentice, I. C., & Pereira, J. M. C. (2013). Relationships between human population density and burned area at continental and global scales. *PLoS One*, 8(12), e81188–12. <https://doi.org/10.1371/journal.pone.0081188>
- Bond, W. J., Woodward, F. I., & Midgley, G. F. (2004). The global distribution of ecosystems in a world without fire. *New Phytologist*, 165(2), 525–538. <https://doi.org/10.1111/j.1469-8137.2004.01252.x>
- Brönnimann, S., Volken, E., Lehmann, K., & Wooster, M. (2009). Biomass burning aerosols and climate—a 19th century perspective. *Meteorologische Zeitschrift*, 18(3), 349–353.
- Cecil, D. J., Buechler, D. E., & Blakeslee, R. J. (2014). Gridded lightning climatology from TRMM-LIS and OTD: Dataset description. *Atmospheric Research*, 135–136, 404–414. <https://doi.org/10.1016/j.atmosres.2012.06.028>

- Chen, Y., Morton, D. C., Jin, Y., Collatz, G. J., Kasibhatla, P. S., van der Werf, G. R., ... Randerson, J. T. (2013). Long-term trends and interannual variability of forest, savanna and agricultural fires in South America. *Carbon Management*, 4(6), 617–638. <https://doi.org/10.4155/cmt.13.61>
- Clark, S. K., Ward, D. S., & Mahowald, N. (2015). The sensitivity of global climate to the episodicity of fire aerosol emissions. *Journal of Geophysical Research: Atmospheres*, 120, 11,589–11,607. <https://doi.org/10.1002/2015JD024068>
- Compo, G. P., Whitaker, J. S., Sardeshmukh, P. D., Matsui, N., Allan, R. J., Yin, X., ... Worley, S. J. (2011). The Twentieth Century Reanalysis project. *Quarterly Journal of the Royal Meteorological Society*, 137(654), 1–28. <https://doi.org/10.1002/qj.776>
- Cruz, M. G., Alexander, M. E., & Wakimoto, R. H. (2005). Development and testing of models for predicting crown fire rate of spread in conifer forest stands. *Canadian Journal of Forest Research*, 35(7), 1626–1639. <https://doi.org/10.1139/x05-085>
- Doerr, S. H., & Santín, C. (2016). Global trends in wildfire and its impacts: Perceptions versus realities in a changing world. *Philosophical Transactions of the Royal Society, B: Biological Sciences*, 371(1696), 20150345–10. doi:<https://doi.org/10.1098/rstb.2015.0345>
- Felsberg, A., Kloster, S., Wilkenskeld, S., Andreas, K., & Lasslop, G. (2017). Lightning forcing in global fire models: The importance of temporal resolution. *Journal of Geophysical Research: Biogeosciences*, 122. <https://doi.org/10.1002/2017JG004080>
- Flanner, M. G., Zender, C. S., Randerson, J. T., & Rasch, P. J. (2007). Present-day climate forcing and response from black carbon in snow. *Journal of Geophysical Research*, 112, D11202. <https://doi.org/10.1029/2006JD008003>
- Flannigan, M. D., Krawchuk, M. A., de Groot, J. W., Wotton, B. M., & Gowman, L. M. (2009). Implications of changing climate for global wildland fire. *International Journal of Wildland Fire*, 18(5), 483–425. <https://doi.org/10.1071/WF08187>
- Gaveau, D. L., Salim, M. A., Hergoualc'h, K., Locatelli, B., Sloan, S., Wooster, M., ... Sheil, D. (2014). Major atmospheric emissions from peat fires in Southeast Asia during non-drought years: Evidence from the 2013 Sumatran fires. *Scientific Reports*, 4(1), 6112. <https://doi.org/10.1038/srep06112>
- Giglio, L., Randerson, J. T., & van der Werf, G. R. (2013). Analysis of daily, monthly, and annual burned area using the fourth-generation global fire emissions database (GFED4). *Journal of Geophysical Research: Biogeosciences*, 118, 317–328. <https://doi.org/10.1002/jgrg.20042>
- Grandey, B. S., Lee, H.-H., & Wang, C. (2016). Radiative effects of interannually varying vs. interannually invariant aerosol emissions from fires. *Atmospheric Chemistry and Physics*, 16(22), 14,495–14,513. <https://doi.org/10.5194/acp-16-14495-2016>
- Gromtsev, A. (2002). Natural disturbance dynamics in the boreal forests of European Russia: A review. *Silva Fennica*, 36(1), 41–55.
- Hansen, M. C., Potapov, P. V., Moore, R., Hancher, M., Turubanova, S. A., Tyukavina, A., ... Townshend, J. R. G. (2013). High-resolution global maps of 21st-century forest cover change. *Science*, 342(6160), 850–853. <https://doi.org/10.1126/science.1244693>
- Hantson, S., Kloster, S., Coughlan, M., Daniau, A., Vanni re, B., Br ucher, T., ... Magi, B. (2016). Fire in the earth system: Bridging data and modeling research. *Bulletin of the American Meteorological Society*, 97(6), 1069–1072. <https://doi.org/10.1175/BAMS-D-15-00319.1>
- Houghton, R. A., Hackler, J. L., & Lawrence, K. T. (1999). The U.S. carbon budget: Contributions from land-use change. *Science*, 285(5427), 574–578. <https://doi.org/10.1126/science.285.5427.574>
- Hurtt, G. C., Chini, L. P., Frolking, S., Betts, R. A., Feddema, J., Fischer, G., ... Wang, Y. P. (2011). Harmonization of land-use scenarios for the period 1500–2100: 600 years of global gridded annual land-use transitions, wood harvest, and resulting secondary lands. *Climatic Change*, 109(1–2), 117–161. <https://doi.org/10.1007/s10584-011-0153-2>
- Jacobson, M. Z. (2014). Effects of biomass burning on climate, accounting for heat and moisture fluxes, black and brown carbon, and cloud absorption effects. *Journal of Geophysical Research: Atmospheres*, 119, 8980–9002. <https://doi.org/10.1002/2014JD021861>
- Kaiser, J. W., Heil, A., Andreae, M. O., Benedetti, A., Chubarova, N., Jones, L., ... van der Werf, G. R. (2012). Biomass burning emissions estimated with a global fire assimilation system based on observed fire radiative power. *Biogeosciences*, 9(1), 527–554. <https://doi.org/10.5194/bg-9-527-2012>
- Kaplan, J. O., Krumhardt, K. M., & Zimmermann, N. E. (2012). The effects of land use and climate change on the carbon cycle of Europe over the past 500 years. *Global Change Biology*, 18(3), 902–914. <https://doi.org/10.1111/j.1365-2486.2011.02580.x>
- Keyantash, J., & Dracup, J. A. (2002). The quantification of drought: An evaluation of drought indices. *Bulletin of the American Meteorological Society*, 83(8), 1167–1180.
- Klein Goldewijk, K., Beusen, A., Doelman, J., & Stehfest, E. (2017). Anthropogenic land use estimates for the Holocene—HYDE 3.2. *Earth System Science Data*, 9(2), 927–953. <https://doi.org/10.5194/essd-9-927-2017>
- Klein Goldewijk, K., Beusen, A., Janssen, P., & P. (2010). Long-term dynamic modeling of global population and built-up area in a spatially explicit way: HYDE 3.1. *The Holocene*, 20(4), 565–573. <https://doi.org/10.1177/0959683609356587>
- Kloster, S., Mahowald, N. M., Randerson, J. T., & Lawrence, P. J. (2012). The impacts of climate, land use, and demography on fires during the 21st century simulated by CLM-CN. *Biogeosciences*, 9(1), 509–525. <https://doi.org/10.5194/bg-9-509-2012>
- Kloster, S., Mahowald, N. M., Randerson, J. T., Thornton, P. E., Hoffman, F. M., Levis, S., ... Lawrence, D. M. (2010). Fire dynamics during the 20th century simulated by the Community Land Model. *Biogeosciences*, 7(6), 1877–1902. <https://doi.org/10.5194/bg-7-1877-2010>
- Knorr, W., Arneth, A., & Jiang, L. (2016). Demographic controls of future global fire risk. *Nature Climate Change*, 6(8), 781–785. <https://doi.org/10.1038/nclimate2999>
- Knorr, W., Kaminski, T., Arneth, A., & Weber, U. (2014). Impact of human population density on fire frequency at the global scale. *Biogeosciences*, 11(4), 1085–1102. <https://doi.org/10.5194/bg-11-1085-2014>
- K ppen, W. (1936). In W. K ppen & G. Geiger (Eds.), *Das geographische System der Klimate, "Handbuch der Klimatologie"* (p. 44). Berlin: 1. C. Gebr. Borntraeger.
- Kottek, M., Grieser, J., Beck, C., Rudolf, B., & Rubel, F. (2006). World map of the K ppen-Geiger climate classification updated. *Meteorologische Zeitschrift*, 15(3), 259–263. <https://doi.org/10.1127/0941-2948/2006/0130>
- Krause, A., Kloster, S., Wilkenskeld, S., & Paeth, H. (2014). The sensitivity of global wildfires to simulated past, present, and future lightning frequency. *Journal of Geophysical Research: Biogeosciences*, 119, 312–322. <https://doi.org/10.1002/2013JG002502>
- Krylov, A., McCrthy, J. L., Potapov, P., Loboda, T., Tyukavina, A., Turubanova, S., & Hansen, M. C. (2014). Fire disturbance and climate change: Implications for Russian forests. *Environmental Research Letters*, 12(3), 035003. <https://doi.org/10.1088/1748-9326/aa5eed>
- Lamarque, J. F., Bond, T. C., Eyring, V., Granier, C., Heil, A., Klimont, Z., ... van Vuuren, D. P. (2010). Historical (1850–2000) gridded anthropogenic and biomass burning emissions of reactive gases and aerosols: Methodology and application. *Atmospheric Chemistry and Physics*, 10(15), 7017–7039. <https://doi.org/10.5194/acp-10-7017-2010>
- Lannom, K. O., Tinkham, W. T., Smith, A. M. S., Abatzoglou, J., Newingham, B. A., Hall, T. E., ... Sparks, A. M. (2014). Defining extreme wildland fires using geospatial and ancillary metrics. *International Journal of Wildland Fire*, 23(3), 322–316. <https://doi.org/10.1071/WF13065>
- Lasslop, G., Brovkin, V., Reick, C. H., Bathiany, S., & Kloster, S. (2016). Multiple stable states of tree cover in a global land surface model due to a fire-vegetation feedback. *Geophysical Research Letters*, 43, 6324–6331. <https://doi.org/10.1002/2016GL069365>

- Lasslop, G., Hantson, S., & Kloster, S. (2015). Influence of wind speed on the global variability of burned fraction: A global fire model's perspective. *International Journal of Wildland Fire*, 24(7), 989–1000.
- Le Page, Y., Morton, D., Bond-Lamberty, B., Pereira, J. M. C., & Hurtt, G. (2015). HESFIRE: A global fire model to explore the role of anthropogenic and weather drivers. *Biogeosciences*, 12(3), 887–903. <https://doi.org/10.5194/bg-12-887-2015>
- Lelieveld, J., Evans, J. S., Fnais, M., Giannadaki, D., & Pozzer, A. (2015). The contribution of outdoor air pollution sources to premature mortality on a global scale. *Nature*, 525(7569), 367–371. <https://doi.org/10.1038/nature15371>
- Li, F., Levis, S., & Ward, D. S. (2013). Quantifying the role of fire in the Earth system—Part 1: Improved global fire modeling in the Community Earth System Model (CESM1). *Biogeosciences*, 10(4), 2293–2314. <https://doi.org/10.5194/bg-10-2293-2013>
- Li, F., Zeng, X. D., & Levis, S. (2012). A process-based fire parameterization of intermediate complexity in a Dynamic Global Vegetation Model. *Biogeosciences*, 9(7), 2761–2780. <https://doi.org/10.5194/bg-9-2761-2012>
- Mahowald, N. M., Ward, D. S., Doney, S. C., Hess, P. G., & Randerson, J. T. (2017). Are the impacts of land use on warming underestimated in climate policy? At Press. *Environmental Research Letters*, 12(9). <https://doi.org/10.1088/1748-9326/aa836d>
- Malyshev, S., Shevliakova, E., Stouffer, R. J., & Pacala, S. W. (2015). Contrasting local versus regional effects of land-use-change-induced heterogeneity on historical climate: Analysis with the GFDL Earth System Model. *Journal of Climate*, 28(13), 5448–5469. <https://doi.org/10.1175/JCLI-D-14-00586.1>
- Marlier, M. E., DeFries, R. S., Kim, P. S., Gaveau, D. L. A., Koplitz, S. N., Jacob, D. J., ... Myers, S. S. (2015). Regional air quality impacts of future fire emissions in Sumatra and Kalimantan. *Environmental Research Letters*, 10(5), 054010. <https://doi.org/10.1088/1748-9326/10/5/054010>
- Marlon, J. R., Bartlein, P. J., Carcaillet, C., Gavin, D. G., Harrison, S. P., Higuera, P. E., ... Prentice, I. C. (2008). Climate and human influences on global biomass burning over the past two millennia. *Nature Geoscience*, 1(10), 697–702. <https://doi.org/10.1038/ngeo313>
- Marlon, J. R., Kelly, R., Daniiau, A.-L., Vanni re, B., Power, M. J., Bartlein, P., ... Zhihai, T. (2016). Reconstructions of biomass burning from sediment charcoal records to improve data-model comparisons. *Biogeosciences*, 13(11), 3225–3244. <https://doi.org/10.5194/bg-13-3225-2016>
- Mieville, A., Granier, C., Lioussse, C., Guillaume, B., Mouillot, F., Lamarque, J.-F., ... Petron, G. (2010). Emissions of gases and particles from biomass burning using satellite data and an historical reconstruction. *Atmospheric Environment*, 44(11), 1469–1477. <https://doi.org/10.1016/j.atmosenv.2010.01.011>
- Millar, C. L., & Stephenson, N. L. (2015). Temperate forest health in an era of emerging megadisturbance. *Science*, 349(6250), 823–826. <https://doi.org/10.1126/science.aaa9933>
- Milly, P. C. D., Malyshev, S. L., Shevliakova, E., Dunne, K. A., Findell, K. L., Gleeson, T., ... Swenson, S. (2014). An enhanced model of land water and energy for global hydrologic and earth-system studies. *Journal of Hydrometeorology*, 15(5), 1739–1761. <https://doi.org/10.1175/JHM-D-13-0162.1>
- Mouillot, F., & Field, C. B. (2005). Fire history and the global carbon budget: A 1x1 fire history reconstruction for the 20th century. *Global Change Biology*, 11(3), 398–420. <https://doi.org/10.1111/j.1365-2486.2005.00920.x>
- Naik, V., Mauzerall, D. L., Horowitz, L. W., Schwarzkopf, M. D., Ramaswamy, V., & Oppenheimer, M. (2007). On the sensitivity of radiative forcing from biomass burning aerosols and ozone to emission location. *Geophysical Research Letters*, 34, L03818. <https://doi.org/10.1029/2006GL028149>
- Nepstad, D. C., Schwartzman, S., Bamberger, B., Santilli, M., Ray, D., Schlesinger, P., ... Rolla, A. (2006). Inhibition of Amazon deforestation and fire by parks and indigenous lands. *Conservation Biology*, 20(1), 65–73. <https://doi.org/10.1111/j.1523-1739.2006.00351.x>
- Nevison, C. D., Mahowald, N. M., Doney, S. C., Lima, I. D., van der Werf, G. R., Randerson, J. T., ... McKinley, G. A. (2008). Contribution of ocean, fossil fuel, land biosphere, and biomass burning carbon fluxes to seasonal and interannual variability in atmospheric CO<sub>2</sub>. *Journal of Geophysical Research*, 6, G01010. <https://doi.org/10.1029/2007JG000408>
- Pechony, O., & Shindell, D. T. (2010). Driving forces of global wildfires over the past millennium and the forthcoming century. *Proceedings of the National Academy of Sciences*, 107(45), 19,167–19,170. <https://doi.org/10.1073/pnas.1003669107>
- Peel, M. C., Finlayson, B. L., & McMahon, T. A. (2007). Updated world map of the K ppen-Geiger climate classification. *Hydrology and Earth System Sciences*, 11(5), 1633–1644. <https://doi.org/10.5194/hess-11-1633-2007>
- Pfeiffer, M., Spessa, A., & Kaplan, J. O. (2013). A model for global biomass burning in preindustrial time: LPJ-LMfire (v1.0). *Geoscientific Model Development*, 6(3), 643–685. <https://doi.org/10.5194/gmd-6-643-2013>
- Rabin, S. S., Magi, B. I., Shevliakova, E., & Pacala, S. W. (2015). Quantifying regional, time-varying effects of cropland and pasture on vegetation fire. *Biogeosciences*, 12(22), 6591–6604. <https://doi.org/10.5194/bg-12-6591-2015>
- Rabin, S. S., Malyshev, S. L., Magi, B. I., Shevliakova, E., & Pacala, S. W. (2017). A fire model with distinct crop, pasture, and non-agricultural burning: Use of new data and a model-fitting algorithm for FINALv1. *Geoscientific Model Development Discussion*, 1–48. <https://doi.org/10.5194/gmd-2017-77>
- Randerson, J. T., Chen, Y., van der Werf, G. R., Rogers, B. M., & Morton, D. C. (2012). Global burned area and biomass burning emissions from small fires. *Journal of Geophysical Research*, 117, G04012. <https://doi.org/10.1029/2012JG002128>
- Real, E., Law, K. S., Weinzierl, B., Fiebig, M., Petzold, A., Wild, O., ... Blake, D. (2007). Processes influencing ozone levels in Alaskan forest fire plumes during long-range transport over the North Atlantic. *Journal of Geophysical Research*, 112, D10541. <https://doi.org/10.1029/2006JD007576>
- Reddington, C. L., Yoshioka, M., Balasubramanian, R., Ridley, D., Toh, Y. Y., Arnold, S. R., & Spracklen, D. V. (2014). Contribution of vegetation and peat fires to particulate air pollution in Southeast Asia. *Environmental Research Letters*, 9(9), 094006. <https://doi.org/10.1088/1748-9326/9/9/094006>
- Rogers, B. M., Soja, A. J., Goulden, M. L., & Randerson, J. T. (2015). Influence of tree species on continental differences in boreal fires and climate feedbacks. *Nature Geoscience*, 8(3), 228–234. <https://doi.org/10.1038/ngeo2352>
- Rothermel, R. C. (1991). Predicting behavior and size of crown fires in the northern Rocky Mountains, Res. Paper INT-438. Ogden, UT: U.S. Dep. of Agriculture, Forest Service, Intermountain Forest and Range Experiment Station, pp. 46.
- Running, S. W. (2006). Is global warming causing more, larger wildfires?. *Science*, 313(5789), 927.
- Sheffield, J., Goteti, G., & Wood, E. F. (2006). Development of a 50-year high-resolution global dataset of meteorological forcings for land surface modeling. *Journal of Climate*, 19(13), 3088–3111. <https://doi.org/10.1175/JCLI3790.1>
- Shevliakova, E., Pacala, S. W., Malyshev, S., Hurtt, G. C., Milly, P. C. D., Caspersen, J. P., ... Crevoisier, C. (2009). Carbon cycling under 300 years of land use change: Importance of the secondary vegetation sink. *Global Biogeochemical Cycles*, 23, GB2022. <https://doi.org/10.1029/2007GB003176>
- Stephens, S. L., Burrows, N., Buyantuyev, A., Gray, R. W., Keane, R. E., Kubian, R., ... van Wagtenonk, J. W. (2014). Temperate and boreal forest mega-fires: Characteristics and challenges. *Frontiers in Ecology and the Environment*, 12(2), 115–122. <https://doi.org/10.1890/120332>

- Stocks, B. J., Mason, J. A., Todd, J. B., Bosch, E. M., Wotton, B. M., Amiro, B. D., ... Skinner, W. R. (2002). Large forest fires in Canada, 1959–1997. *Journal of Geophysical Research*, 108(D1), 8149. <https://doi.org/10.1029/2001JD000484>
- Stocks, B. J., Wotton, B. M., Flannigan, M. D., Fosberg, M. A., Cahoon, D. R., & Goldammer, J. G. (2001). Boreal forest fire regimes and climate change. In M. Beniston & M. M. Verstraete (Eds.), *Remote sensing and climate modeling: Synergies and limitations* (pp. 233–246). The Netherlands. [https://doi.org/10.1007/0-306-48149-9\\_10](https://doi.org/10.1007/0-306-48149-9_10)
- Sulman, B. N., Phillips, R. P., Oishi, A. C., Shevliakova, E., & Pacala, S. W. (2014). Microbe-driven turnover offsets mineral-mediated storage of soil carbon under elevated CO<sub>2</sub>. *Nature Climate Change*, 4(12), 1099–1102. <https://doi.org/10.1038/nclimate2436>
- Thonicke, K., Spessa, A., Prentice, I. C., Harrison, S. P., Dong, L., & Carmona-Moreno, C. (2010). The influence of vegetation, fire spread and fire behaviour on biomass burning and trace gas emissions: Results from a process-based model. *Biogeosciences*, 7(6), 1991–2011. <https://doi.org/10.5194/bg-7-1991-2010>
- van der Werf, G. R., Peters, W., van Leeuwen, T. T., & Giglio, L. (2013). What could have caused pre-industrial biomass burning emissions to exceed current rates? *Climate of the Past*, 9(1), 289–306. <https://doi.org/10.5194/cp-9-289-2013>
- van der Werf, G. R., Randerson, J. T., Collatz, G. J., Giglio, L., Kasibhatla, P. S., Arellano, A. F., ... Kasischke, E. S. (2004). Continental-scale partitioning of fire emissions during the 1997–2001 El Niño/La Niña period. *Science*, 303(5654), 73–76. <https://doi.org/10.1126/science.1090753>
- van der Werf, G. R., Randerson, J. T., Giglio, L., Collatz, G. J., Kasibhatla, P. S., & Arellano, A. F. Jr. (2006). Interannual variability in global biomass burning emissions from 1997 to 2004. *Atmospheric Chemistry and Physics*, 6(11), 3423–3441. <https://doi.org/10.5194/acp-6-3423-2006>
- van der Werf, G. R., Randerson, J. T., Giglio, L., Collatz, G. J., Mu, M., Kasibhatla, P. S., ... van Leeuwen, T. T. (2010). Global fire emissions and the contribution of deforestation, savanna, forest, agricultural, and peat fires (1997–2009). *Atmospheric Chemistry and Physics*, 10(23), 11,707–11,735. <https://doi.org/10.5194/acp-10-11707-2010>
- van Marle, M. J. E., Kloster, S., Magi, B. I., Marlon, J. R., Daniiau, A.-L., Field, R. D., ... van der Werf, G. R. (2017). Historic global biomass burning emissions for CMIP6 (BB4CMIP) based on merging satellite observations with proxies and fire models (1750–2015). *Geoscientific Model Development*, 10(9), 3329–3357. <https://doi.org/10.5194/gmd-10-3329-2017>
- Veraverbeke, S., Rogers, B. M., Goulden, M. L., Jandt, R. R., Miller, C. E., Wiggins, E. B., & Randerson, J. T. (2017). Lightning as a major driver of recent large fire years in North American boreal forests. *Nature Climate Change*, 7(7), 529–534. <https://doi.org/10.1038/nclimate3329>
- Virts, K. S., Wallace, J. M., Hutchins, M. L., & Holzworth, R. H. (2013). Highlights of a new ground-based, hourly global lightning climatology. *Bulletin of the American Meteorological Society*, 94(9), 1381–1391. <https://doi.org/10.1175/BAMS-D-12-00082.1>
- Voulgarakis, A., & Field, R. D. (2015). Fire influences on atmospheric composition, air quality and climate. *Current Pollution Reports*, 1(2), 70–81. <https://doi.org/10.1007/s40726-015-0007-z>
- Voulgarakis, A., Marlier, M. E., Faluvegi, G., Shindell, D. T., Tsigaridis, K., & Mangeon, S. (2015). Interannual variability of tropospheric trace gases and aerosols: The role of biomass burning emissions. *Journal of Geophysical Research: Atmospheres*, 120, 7157–7173. <https://doi.org/10.1002/2014JD022926>
- Wang, X., Parisien, M.-A., Flannigan, M. D., Parks, S. A., Anderson, K. R., Little, J. M., & Taylor, S. W. (2014). The potential and realized spread of wildfires across Canada. *Global Change Biology*, 20(8), 2518–2530. <https://doi.org/10.1111/gcb.12590>
- Wang, X., Parisien, M.-A., Taylor, S. W., Candau, J.-N., Stralberg, D., Marshall, G. A., ... Flannigan, M. D. (2017). Projected changes in daily fire spread across Canada over the next century. *Environmental Research Letters*, 12(2), 025005–13. <https://doi.org/10.1088/1748-9326/aa5835>
- Ward, D. S., Kloster, S., Mahowald, N. M., Rogers, B. M., Randerson, J. T., & Hess, P. G. (2012). The changing radiative forcing of fires: Global model estimates for past, present and future. *Atmospheric Chemistry and Physics*, 12(22), 10,857–10,886. <https://doi.org/10.5194/acp-12-10857-2012>
- Ward, D. S., & Mahowald, N. M. (2015). Local sources of global climate forcing from different categories of land use activities. *Earth System Dynamics*, 6(1), 175–194. <https://doi.org/10.5194/esd-6-175-2015>
- Ward, D. S., Shevliakova, E., Malyshev, S., Lamarque, J.-F., & Wittenberg, A. T. (2016). Variability of fire emissions on interannual to multi-decadal timescales in two Earth System models. *Environmental Research Letters*, 11(12), 125008. <https://doi.org/10.1088/1748-9326/11/12/125008>
- Wiedinmyer, C., Akagi, S. K., Yokelson, R. J., Emmons, L. K., Al-Saadi, J. A., Orlando, J. J., & Soja, A. J. (2011). The fire inventory from NCAR (FINN): A high resolution global model to estimate the emissions from open burning. *Geoscientific Model Development*, 4(3), 625–641. <https://doi.org/10.5194/gmd-4-625-2011>
- Wooster, M. J., & Zhang, Y. H. (2004). Boreal forest fires burn less intensely in Russia than in North America. *Geophysical Research Letters*, 31, L20505. <https://doi.org/10.1029/2004GL020805>
- Yang, J., Tian, H., Tao, B., Ren, W., Kush, J., Liu, Y., & Wang, Y. (2014). Spatial and temporal patterns of global burned area in response to anthropogenic and environmental factors: Reconstructing global fire history for the 20th and early 21st centuries. *Journal of Geophysical Research: Biogeosciences*, 119, 249–263. <https://doi.org/10.1002/2013JG002532>
- Yue, C., Ciais, P., Cadule, P., Thonicke, K., Archibald, S., Poulter, B., ... Viovy, N. (2014). Modeling the role of fires in the terrestrial carbon balance by incorporating SPITFIRE into the global vegetation model ORCHIDEE—Part 1: Simulating historical global burned area and fire regimes. *Geoscientific Model Development*, 7(6), 2747–2767. <https://doi.org/10.5194/gmd-7-2747-2014>
- Yue, C., Ciais, P., Cadule, P., Thonicke, K., & van Leeuwen, T. T. (2015). Modeling the role of fires in the terrestrial carbon balance by incorporating SPITFIRE into the global vegetation model ORCHIDEE—Part 2: Carbon emissions and the role of fires in the global carbon balance. *Geoscientific Model Development*, 8(5), 1321–1338. <https://doi.org/10.5194/gmd-8-1321-2015>